UNIVERSIDADE FEDERAL DE MINAS GERAIS

Instituto de Geociências

Programa de Pós-Graduação em Geologia

Maria José Campos de Oliveira

3D CHARACTERIZATION OF THE MAGNETIC RESPONSE OF THE AIMORÉS INTRUSIVE COMPLEX (BRAZIL): COMPARISON WITH IMPACT STRUCTURES

Nº 225

Belo Horizonte
DATA 17/05/2021

Maria José Campos de Oliveira

3D CHARACTERIZATION OF THE MAGNETIC RESPONSE OF THE AIMORÉS INTRUSIVE COMPLEX (BRAZIL): COMPARISON WITH IMPACT STRUCTURES

Versão Final

Dissertação apresentada ao programa de Pós-Graduação em Geologia do Instituto de Geociências da Universidade Federal de Minas Gerais como requisito para obtenção do título de mestre em Geologia.

Área de Concentração: Geologia Regional

Orientador: Prof.ª. Dr.ª Aline Tavares Melo

Coorientador: Prof. Dr. Marcos Alberto Rodrigues Vasconcelos

Belo Horizonte

2021

O48c Oliveira, Maria José Campos de.
2021 3D characterization of the magnetic response of The Aimorés Instrusive Complex (Brazil) [manuscrito] : comparison with impact structures / Maria José Campos de Oliveira. – 2021.
xxiv, 55 f., enc.: il. (principalmente color.)

Orientadora: Aline Tavares Melo.
Coorientador: Marcos Alberto Rodrigues Vasconcelos .
Dissertação (mestrado) – Universidade Federal de Minas Gerais, Instituto de Geociências, 2021.
Área de concentração: Geologia Regional.
Bibliografia: f.47-55.

1. Geofísica – Teses. 2. Susceptibilidade magnética – Teses. I. Melo, Aline Tavares. II. Vasconcelos, Marcos Alberto Rodrigues. III. Universidade Federal de Minas Gerais. Instituto de Geociências. IV. Título.

CDU: 550.3

Ficha catalográfica elaborada por Graciane Aparecida de Paula – CRB6 3404

UNIVERSIDADE FEDERAL DE MINAS GERAIS

PROGRAMA DE PÓS-GRADUAÇÃO EM GEOLOGIA

FOLHA DE APROVAÇÃO

3D characterization of the magnetic response of the Aimorés Intrusive Complex (Brazil): comparison with impact structures

MARIA JOSÉ CAMPOS DE OLIVEIRA

Dissertação submetida à Banca Examinadora designada pelo Colegiado do Programa de Pós-Graduação em GEOLOGIA, como requisito para obtenção do grau de Mestre em GEOLOGIA, área de concentração GEOLOGIA ECONÔMICA E APLICADA.

Aprovada em 17 de maio de 2021, pela banca constituída pelos membros:

Profa. Aline Tavares Melo - Orientadora
UFMG

Prof. Emilson Pereira Leite
Unicamp

Profa. Marilane Gonzaga de Melo
UFES

Belo Horizonte, 17 de maio de 2021.

Acknowledgments

I am sincerely grateful for all the help and contributions received during these two years of research.

- Firstly, I want to thank both my mentors, professor Aline Melo and professor Marcos Vasconcelos for their unwavering support, valuable discussions, knowledge shared and and the motivating enthusiasm;
- This master's project was only possible due to the support of the Graduate Geology Program at the Institute of Geosciences (IGC) of the Universidade Federal de Minas Gerais (UFMG) and the Geology Department of Universidade Federal da Bahia (UFBA);
- My colleagues Mariana Bandeira and Tobias Fonte Boa for all the discussions in our study group, that were of essential value for this research;
- I thank Marco Couto, researcher of CPRM, for sharing his knowledge in inversion theory and for technical support;
- I would also like to thank my colleagues for the discussions on the office of the graduate students at the Geosciences Institute;
- Finally, I am forever grateful to my family and friends, this research was only made possible due to their love, comprehension and emotional support.

I'm thankful to God Almighty
protector of my whole life!

Maria José

Resumo

O orógeno Araçuaí é uma importante região para a história geológica do Brasil, e por anos tem sido estudado os mecanismos geotectônicos da área para elucidar a produção extensa das rochas graníticas que ocorrem na região. Os pulsos magmáticos que formaram o orógeno, o subdividiram em supersuites G1, G2, G3, G4 e G5, que são responsáveis por marcar estágios geotectônicos específicos. O Complexo Intrusivo de Aimorés é um representante dos corpos graníticos intrusivos característico da supersuite G5, de caráter pós-collisional, relacionado ao clímax do colapso gravitacional do orógeno. O Complexo Intrusivo de Aimorés apresenta feição circular, característica de uma estrutura formada por um impacto de um meteoro. Sua expressão morfológica em superfície fez com que a região ficasse reconhecida localmente como "cratera de impacto de Aimorés". O processo de modificação da superfície do planeta através do impacto de corpos extraterrestres é bastante comum e seus registros geológicos são conhecidos como crateras de impacto. A identificação correta de uma cratera depende de uma série de critérios geológicos específicos, e uma investigação inicial é possível através de estudos geofísicos. O objetivo deste trabalho é caracterizar a assinatura geofísica do Complexo de Aimorés em 3D, entender a geometria das diferentes zonas litológicas e compara suas assinaturas com outras crateras existentes. A metodologia proposta é efetuada através da integração de dados geológicos para gerar um modelo de inversão magnética satisfatório de ser interpretado. A inversão do campo anômalo magnético identificou uma área de baixa susceptibilidade ao redor da intrusão ígnea de aimorés, correspondente às rochas encaixantes sin-colisionais da super suíte G2. Foram identificadas também duas zonas de alta susceptibilidade coincidentes com a região de ocorrência das rochas pós-colisionais do G5, O complexo intrusivo de Aimorés, e também o complexo intrusivo de Urucum. A resposta magnética de Aimorés é diferente da que é esperada de crateras de impacto com morfologia e diâmetro similares. Deste modo, neste trabalho mostramos que estruturas com características similares em superfície podem ter diferente geometria em subsuperficie.

Palavras-chave: Geofísica Aplicada, Inversão Magnética, Complexo Intrusivo de Aimorés.

Abstract

The Araçuaí orogen is an important region for Brazil's geological history, and for years the geotectonic mechanisms of the area have been studied to elucidate the extensive production of granitic rocks that occur in the site. The magmatic pulses that build the orogen, subdivided it into supersuites G1, G2, G3, G4, and G5, and mark specific geotectonic stages. The Aimorés Igneous Complex (AIC) is one representative of the intrusive granitic bodies from the supersuite G5, post-collisional, related to the gravitational collapse of the orogen. The AIC shows a circular morphology that reassembles a structure formed through a cratering process. Its morphological expression on surface made the region be recognized locally as "Aimorés impact crater". It is well known that the more common process of alteration and modification of Earth's surface is the impact of extraterrestrial bodies, and the geological register of such event is known as impact craters. The correct identification of a crater depends on a number of specific geological criteria, but an initial investigation is possible using tools such as geophysics. Therefore, the main goal of the present work is to characterize the geophysical signature of the Aimorés Complex in 3D, understand the geometry of the different lithological zones, and compare their signature with other existing craters. The proposed methodology is carried out through the integration of geological data to generate a satisfactory magnetic inversion model to be interpreted. The inversion of the magnetic susceptibility identified an area of low susceptibility around the igneous intrusion of Aimorés, corresponding to the syn-collisional host rocks of the G2 supersuite. Two areas of high susceptibility are coincident with the region of occurrence of the G5 post-collisional rocks were also identified, the intrusive complex of Aimorés, and also, the intrusive complex of Urucum. It is observed that the magnetic response of the CIA is different from that expected of impact craters with similar morphology and diameter. Thus, in this work we show that structures with similar characteristics on the surface can have different subsurface geometry and geophysical signatures.

Keywords: Applied Geophysics, Magnetic Inversion, Aimorés Intrusive Complex.

"It is important to draw wisdom from many different places... If we take it from only one place it becomes rigid and stale."

Uncle Iroh

Table of Figures

Figure **Page**

Table of Nomenclatures

α_s	Component coefficient.
α_x	Component coefficient in x.
α_y	Component coefficient in y.
α_z	Component coefficient in z.
β	Regularization parameter.
δ	Data observed minus data predicted.
η	Measurements errors.
ϕ_d	Data misfit.
ϕ_m	Model norm.
b_l	Lower bound.
b_u	Upper bound.
d	Data.
d	Magnetic vector.
d^{obs}	Data observed.
F	Forward operator.
$G1$	Pre-collisional supersuite.
$G2$	Syn-collisional supersuite.
$G3$	Late-collitional supersuite.

$G4$ Late-collitional supersuite.

$G5$ Post-collisional supersuite.

H Geomagnetic field.

k Magnetic susceptibility.

m Susceptibility vector.

m_0 Reference model.

$w(z)$ Depth weighting function.

W_s Spatially dependent weighting function.

W_x Spatially dependent weighting function in x.

W_y Spatially dependent weighting function in y.

W_z Spatially dependent weighting function in z.

Table of Abbreviations

AIC	Aimorés Intrusive Complex
CPRM	Brazilian Geological Service
MME	National Mines and Energy Ministry
IGRF	International Geomagnetic Reference Field
TMI	Total Magnetic Intensity

Table of Contents

CHAPTER 1

Introduction

Orogenic Belts are regions that records extensive granite production during its geotectonic states, and one important representative is the Araçuaí orogen, located in the southeast portion of the Brazilian territory, which is a confined terrain surrounded by cratonic landmasses (Alkmim *et al.*, 2006, 2017; Pedrosa-Soares *et al.*, 2001, 2008, 2011a). The orogen granite production represents events from the pre-collisional to the latest post-collisional stages. And there is an important link between the type of the magmatism and the correspondent tectonic stage of the orogen (Chappel and White, 1974, 2001). Within the granitic rocks it is possible to distinguish distinct petrologic signatures which represents each tectonic stage: pre-collisional, collisional and post-collisional. The pre-collisional granitic rocks are associated with the lithosphere subduction and are well represented by normal calc-alkalic, I-type granitoids that indicates the development of volcanic arcs in oceanic or continental active margin settings. (Pitcher, 1993; Cobbing, 1996; Pearce, 1996). Meanwhile the collisional, or syn-collisional granites are linked with crustal thickening generally by the under thrusting of one crustal slab beneath another (Harris *et al.*, 1986). They correspond to the peraluminous type-S granitoids that often results from extensive sediment subduction into the mantle, or incorporation of the crustal melt into the mantle wedge. These rocks are formed under the temperature rise during this stage, due to the partial melting of recycled sediments by ultrametamorphic anatexis (Pedrosa-Soares *et al.*, 1998), and at last there are the post-collisional granitoids that form after the collision stage is over, these rocks are related to the subsequent collapse of the orogen (Harris *et al.*, 1986; Pitcher, 1993; Pearce,

1996). Post-collisional granitoids generally show no penetrative, ductile tectonic foliation, forming roughly circular plutons with the pre-existing regional structures accommodated around them. These rocks are High-K calc-alkalic, I-type granites to tonalites. The peraluminous, subalkalic to alkalic S-type leucogranites are also granitoids from this geotectonic stage. (Pitcher, 1993; Roberts and Clemens, 1993; Pearce, 1996). Type-I granites that are associated with a distensile tectonic setting (Pedrosa-Soares *et al.*, 2011b). The Late Neoproterozoic-Cambrian Araçuaí orogen, as previously said, records extensive granite production into granitoid supersuites (G1, G2, G3, G4, and G5), correspondent to each of the tectonic stages of the orogen (Alkmim *et al.*, 2006, 2017; Pedrosa-Soares *et al.*, 2001, 2008, 2011a).

Aimorés Igneous Complex (AIC) has topographical features that resemble an impact structure, such: (*i*) its circular shape; (*ii*) raised arched edges; (*iii*) depressed central part; (*iv*) centrifugal drainage pattern (Hachiro and Fernandez, 2004), and on satellite images it is possible to identify the crateriform circular shape. For this reason, the structure has been listed as a possible impact structure in Brazil on the Expert Database on Earth Impact Structures (EDEIS). However, other petrographic evidences are necessary to prove this sort of origin. But they have not been found in Aimorés. On the other hand, detailed geological mapping of Aimorés region confirmed that it is a one of the granitic intrusions of the G5 supersuite, classified as a post-collisional plutonic body intruded into G2 sin-collisional rocks (Pedrosa-Soares *et al.*, 2011a). Therefore, here we refer as the Aimorés Intrusive Complex (AIC).

Aimorés has all topographical features of such structure and we would like to investigate if its geophysical signature in 2D and 3D is also similar to an impact crater. The understanding of the similarities and differences of the geophysical response between Aimorés and proven impact structures will help elucidate if magnetic data can be used as a tool to distinguish between these structures with similar terrain morphology. The impact of celestial bodies is recognized as the main modification process of planetary bodies surfaces in the solar system (Koeberl, 2001), including planet Earth. Astroblemes, a term proposed by Dietz (1969), or impact craters as they are known, mark the testimony of the impact in form of scars on the earth's surface, however these features are hardly identified, given the processes of erosion, sedimentation and tectonic movement that bury or erase the records of these impact events (Crósta, 2012). There are many features that are not specifically characteristic features of impact structures, so the correct identification is based on a set of metamorphic effects, often expressed in microscopic forms for example as planar deformation features in grains of quartz, that are the unique products of impact-

produced shock waves (French, 1968a; French and Short, 1968; French, 1998; Koeberl and Shirey, 1991; Koeberl, 2002; Langenhorst, 2002). The tools used to distinguish an impact structure from other features formed by endogenous geological processes are critical to understand the origin of structures that show similar morphological expressions. Geophysics is frequently used to identify and explain such structures. And, because Aimorés is listed as a possible impact structure, we decided to analyze the magnetic data and build a 3D model as well.

Through the analysis of the magnetic data and the inversion of magnetic susceptibility, we imaged the geometry of the AIC at depth to investigate the difference from an impact crater. I made surface 2D interpretations of the AIC magnetic data, as well as interpretations of 3D susceptibility models of the subsurface. It was performed 3D inversions of magnetic susceptibility data in order to achieve the best model to understand the geometry of the AIC. In this study, we propose a method to integrate prior lithology information as a constraint to geophysical modeling and compare it to geophysical responses of impact structures to elucidate if different geological structures could have similar geophysical responses.

The first chapter shows the location of the AIC; its geological setting and the methodology used in the inversion. The second chapter presents the manuscript that is the main part of the dissertation and contains the geophysical analysis of the AIC, inversion results, discussions and conclusions achieved. Finally, the third chapter brings suggestions for future works.

CHAPTER 2

Area of study and fundamentals

2.1 Location, access, geological setting and methods

The Aimorés Intrusive Complex (AIC) is located on the border of Minas Gerais state, near Espírito Santo state. The region is characterized by a tropical climate with average temperatures of 24^o to 35^o degrees Celsius and an annual rainfall around of 1500mm. The area of study is located in the municipality of Aimorés, 475 kilometers from the state's capital, Belo Horizonte. The area can be accessed through the BR-259 and BR-381 roads (Figure 2.1).

To illustrate the main geological units the geological mapping made by the Geological Service of Brazil CPRM in an association with the state's secretariat of mines and energy of Minas Gerais is displayed on Figure 2.2. The AIC is represented by the Paleozoic units Caladão granite and Padre Paraíso charnockite. The map is in a 1:100000 scale over the Conselheiro Pena map (SE-24-Y-C-II), and over the Minas Gerais portion of the São Gabriel da Palha mapa (SE-24-Y-C-III).

Figura 2.1: Access image of the study area.

2.2 Geological setting of the Aimorés Intrusive Complex

The annular multi-intrusive Aimorés Intrusive Complex has approximately 150 km^2 of area, and locally has been denominated as an impact structure due to its crateriform expressions. The region raised arched edges, depressed central part, and circular shape of approximately 10 km in diameter contributes to the popular name "Aimorés crater". In 2015, there was a dam breakage in Mariana, Minas Gerais, a city 371 kilometers away from Aimorés's city. The mud debris flow that escaped after the dam's disruption, followed the course of the Doce River, an important drain of Minas Gerais state, that passes right beside the Aimorés structure. For a while, it was a topic of discussion if there was a possibility to divert the mud flow into the "Aimorés Crater", the name used in the media to refer to the AIC low topographic expression.

But the discussion about the possible impact origin of the Aimorés's site goes back in time to 2004, when Hachiro and Fernandez (2004) raised several observations

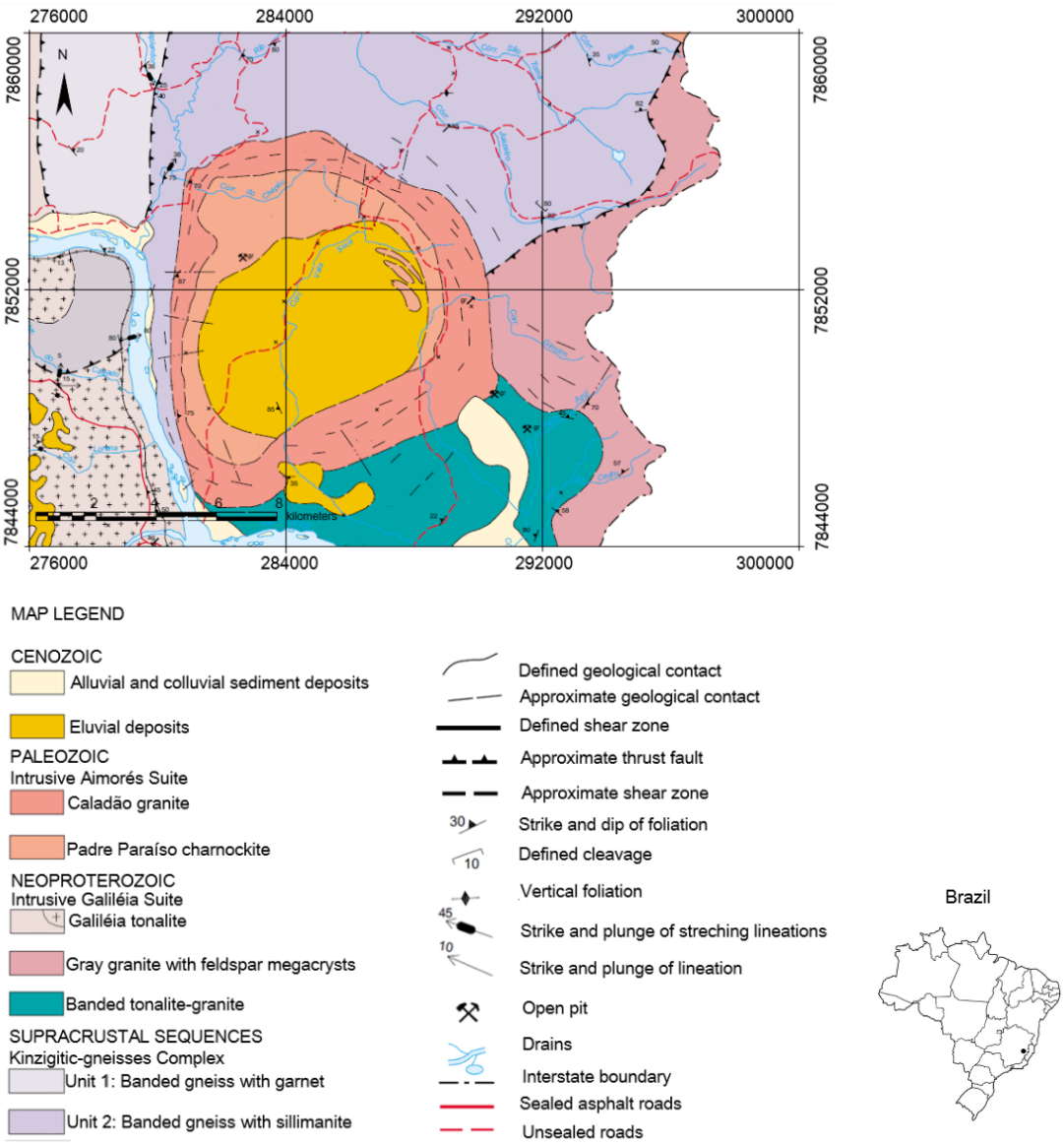

Figura 2.2: a) Simplified geologic map of the AIC. Modified from the Conselheiro Pena map and São Gabriel da Palha map over the Minas Gerais state. b) Representation of Brazil's territory.

Source: adapted from CPRM (2010).

on the structure that could be indicative of an impact origin. They proposed that the circular morphology, the depressed central part, the planar deformation features in some quartz grains, among other features, were indicatives of the impact. However, detailed mapping and geologic analysis over the years in that region show that it is an igneous structure than anything else. The complex consists of basic and intermediate rocks in its central part and progressively more acidic rocks towards the edges. Due to its petrological signatures, it is observed that it resembles similar G5 intrusions that occur all over the Araçuaí orogen, and it is a zoned post-collisional intrusive body, as others representatives of this tectonic stage (Mello, 2011). Mello (2011) performed a characterization of the AIC as a structure with high-angled edges that dips towards the center and shows magmatic flow foliation in its porphyritic granodiorites.

The present work is the first to perform a geophysical inversion modeling over the AIC, and the main objective is to improve the understanding of the structure at depth. But first, it is necessary to understand the background of how the impact structures are formed, in order to understand why Aimorés can not fall into this category of geologic processes that modify the Earth's surface. The second step is to contextualize the methodology used to perform the geophysical analysis of its signature.

2.3 Geophysics of impact craters

The most frequent process of surface modification on several solid planets is the impact of celestial bodies (Koeberl, 2001). But the record of such events is quite often erased because of geological activities such as weathering and plate tectonics on Earth's surface. The ability to distinguish an impact structure from other features formed by endogenous geological processes is a critical factor for knowledge advancement in this area. The indicators of an impact event are found in the target rocks that have undergone extreme temperature and pressure change due to the shock waves generated by the impact (Melosh, 1989). These include crateriform morphology, circular drainage patterns, huge expression of igneous rocks, deformations in local lithologies, and circular geophysical anomalies. The general rule is that impact craters can be recognized and confirmed with certainty only by petrographic criteria and structural evidence, but tools such as geophysical analysis, although not conclusive, are fundamental for the beginning of the study.

(French and Koeberl, 2010) compilated several general principles for recognition and searching of such impact structures: (1) Any circular feature on the earth's surface is more likely to be anything else than an impact structure since geological processes occurring on the earth's surface place a strong role on the record of these terrestrial impact structures, making them quite rare (Trefil and Raup, 1990; Grieve, 1991, 1998). (2) Distinctive deformation features such as shock effects occur over a relatively small and specific area (Ludka *et al.*, 1965; Grieve, 1991). (3) Positive confirmation of such structure can only come from petrographic and geochemical evidence in the rocks. (4) Remote-sensing and geophysical observations are very relevant to initial searches, but by themselves, they can not provide conclusive evidence. (Grieve, 1991; Koeberl, 1997; Grieve, 1998; French, 1998; Koeberl *et al.*, 2004; French, 2005). (5) And at least, fieldwork, sample collecting, and examination are essential.

To understand the geophysical signatures of terrestrial impact craters, we must define the main morphologies: simple and complex (French, 1998). There is a third type called multi-ring basin. It is quite simple to distinguish simple from complex craters, however, the definition of multi-ring crater brings some discussion. Melosh (1989) described them as resulting from different processes to the ones that result in the simple or complex craters, and also, they are most likely to be found in other planetary bodies.

Simple craters are bowl-shaped with parabolic longitudinal profiles and are often smaller when compared to the complex ones. The apparent floor of the crater is underlain by a layer of material, called allochthonous breccia, that has fallen back into the cavity after the impact explosion. The true floor, on the other hand, is where the fractured and brecciated, but in-situ rocks are, it lies under the layer of allochthonous breccia described before. Regarding the raised rim of the crater, when preserved, it displays an overturned stratigraphy due to the rapid excavation of the cavity (Melosh, 1989; Grieve *et al.*, 2010). Complex craters are wider and can be differentiated based on their internal morphology, characterized by a central core raised in relation to its floor, shallower crater floors, and gravitational collapse terraces at the rim. The central peak at the center of the cavity is due to a rebound of the true crater floor. The gravitational collapse of the walls of the excavated cavity produces terraced terrains, this process results in a complex structure wider and shallower than the simple one (Melosh, 1989). Figure 2.3 shows the cross-section of these two morphology types.

The impact that creates the craters is the catalyzer of structural, morphological, and mineralogical changes in the target rocks. It can also change the density and magnetic

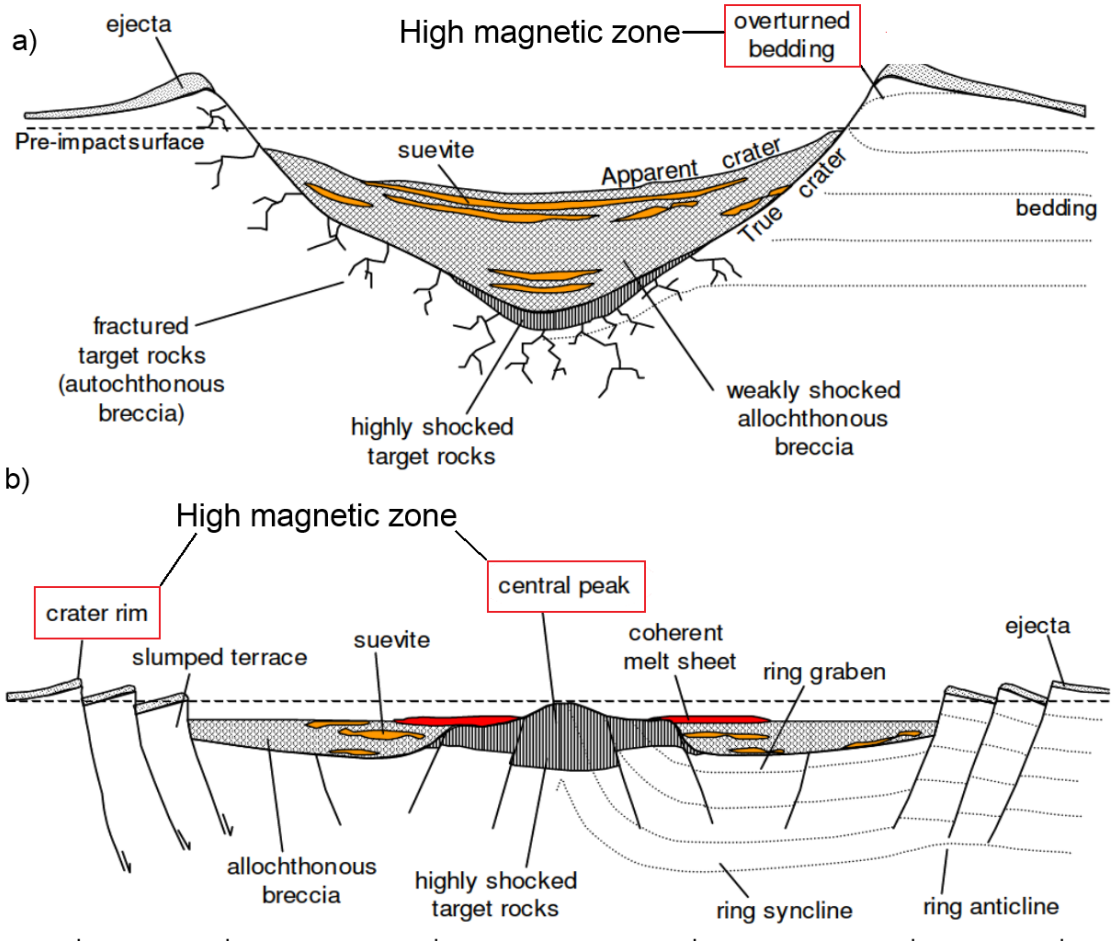

Figura 2.3: a) Schematic cross-section of a simple impact crater. b) Schematic cross-section of a complex impact crater structure.

Source: adapted from Grieve *et al.* (2010) In: Hawke (2004).

susceptibility of such target rocks. These alterations in the petrophysical properties can be quantified using a suitable geophysical technique. These properties contrast between different types of rocks is used to understand the internal geometry of the crater without the need for drilling, for example, and also to bring to light the structures that could have been buried by post-impact sedimentation processes.

The most common geophysical signature of these structures is the circular gravity low that extends to the crater's edge or could go just a little beyond it. These anomalies are observed due to the lateral density contrast with the target rocks and are mainly caused due to the lithological and physical changes associated with the impact process (Pilkington and Grieve, 1992). The famous Chicxulub crater, located at the Yucatan

peninsula in Mexico, shows a typical negative response, more specifically 170km diameter circular gravity low, which correlates with the rim location of the crater (Hidebrand *et al.*, 1991). Gravity methods proved to be efficient to measure the diameter of the crater rim that can be identified by the extent of the gravity low, and even to estimate the depth extent of deformation and amount of structural uplift that has occurred (Pleiscia, 2003). According to Pilkington and Grieve (1992), the peak amplitude of the negative gravity anomaly generally increases with the structure size, up to a maximum of about 30nGal at a 30km diameter.

The magnetic signatures of impact structures are varied and quite complex due to the greater variation in the magnitude of the magnetic properties of the target rocks (Pilkington and Grieve, 1992). The characteristic signature is the magnetic low on the center of the structure in simple craters, and a high magnetic anomaly on the edges easily observed in crystalline environments, that is recognizable by the disruption of the magnetic regional trends (Dabizha and Fedynsky, 1975; Clark, 2001), also a positive anomaly over the central uplift in complex structures (Pilkington and Grieve, 1992). Studies have shown that shock pressures of 1GPa are enough to remove magnetic remanence, and 10GPa can reduce magnetic susceptibility (Pilkington e Grive, 1992). These shock pressures are restricted to smaller areas inside the cavity. weakly magnetic post-impact allochthonous breccia can contribute to the magnetic response, and local high magnetic anomalies can also be found near the center of the structure, because of magnetized components from the basement lithologies that are uplifted at the center of wider structures, this type of magnetization can be classified as “high-frequency” indicating a shallow magnetic source. Or they can be rocks fused by impact or related with thermal, chemical or shock processes, forming new magnetic minerals or resetting the magnetism of target rocks (Pilkington and Grieve, 1992).

The AIC displays a crateriform topographic expression, but detailed mapping shows that it is a zoned igneous body that was intruded during the post-collisional events related to the Araçuaí orogen. In this study, we want to observe Aimorés’s geophysical response and through the investigation of the susceptibility distribution in-depth see if it resembles what is expected of an impact structure.

2.4 Method

In this section I will discuss the methodology applied in order to perform the qualitative interpretations, and geophysical inversions.

2.4.1 Data interpretation

The interpretation of geological structures through geophysical methods is an important tool for many branches of geology from exploration of mineral resources to management of land use in the most diverse environments. Airborne geophysical data have been heavily used as a tool to comprehend the geological structures in subsurface as well as to better interpret the surface relations among the different lithologies. The magnetometric interpretation over the thematic maps on which qualitative analyses were performed, provided the first information about the behavior of the structure in the subsurface. Furthermore, the integration of 2D interpretation with detailed geological mapping substantially increases the area background knowledge. Analyzing spatial variations on Earth's magnetic field is a fundamental step to make a geologically meaningful interpretation of the potential field.

2.4.2 Geophysical inversion theory

Geophysics has always been used to decode geoscience issues. Frequently, we want to characterize the physical property of the geological structure to be recognized, for example: density, magnetic susceptibility, or seismic velocity through a geophysical survey. When the information required to solve the problem is located on the subsurface, the initial step is to model the problem, find a function so that the data can be inverted to generate a 3D model distribution of the physical property to be interpreted (Figure 2.4). For example, to solve the "issue" proposed in this work, we need to invert the data, considering the magnetic field anomaly map of the area to discover the possible distribution of the magnetic susceptibility in depth and build an interpretable model.

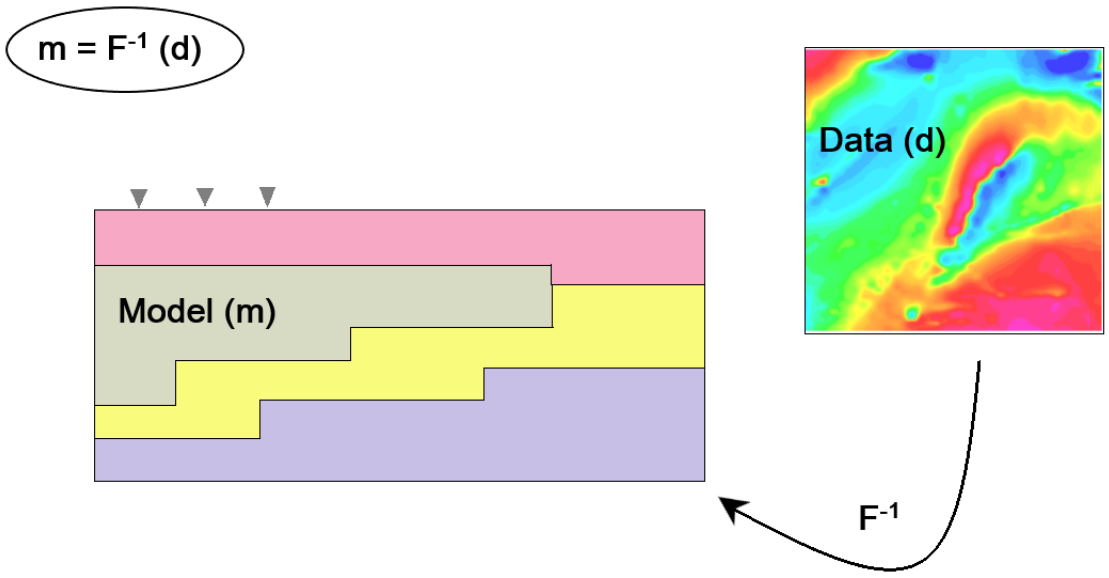

Figura 2.4: Schematic image of the inversion problem. We record data d and predict model m.

The reasons to invert the geophysical data are numerous. It provides the understanding of complex data sets and explain them with a quantitative model that can be analyzed. It also allows to answer questions such as: what is the depth, physical property, volume and geometry of the geological structure investigated? What geologic features can be determined in the model obtained? Furthermore, it allows to separate the noise from the signal in the data and therefore, estimate the noise levels. So, in order to understand the inverse problem in depth we must first understand its fundamentals.

2.4.3 Fundamentals of the inversion

This section of the dissertation was written based on the work of Li and Oldenburg (1996). The two main types of modelling existent are the forward modelling and the inversion. The forward modelling is when it is given a model and we predict the data. It can be written as:

$$d = F(m). \tag{2.1}$$

Where m is the model, d is the data and F is an operator that represents the governing equations according to the data and model in question. On the other side, the

inversion problem is when the data is recorded and we predict a model. It can be written as:

$$m = F^{-1}(d). \tag{2.2}$$

In geophysical inversion, we want to recover physical properties information, such as the magnetic susceptibility for example, from the observed data d. Thus, to start the inversion process it is given the field observations (d), the error estimates, and other prior knowledge about the area we want to perform the inversion on.

The next step is to discretize the Earth over the area we want to perform the inversion. The goal of this work is to invert magnetic data over the Aimorés Intrusive Complex; therefore, we are going to divide the are in rectangular cells in a 3D mesh that assumes a constant magnetic susceptibility (k) for each cell. The magnetization is considered to be uniform for each cell, and can be defined as the product of k and the geomagnetic field H. The correlation between the anomaly observed on the surface with the susceptibility od each cell on subsurface is given by:

$$d = \mathbf{G}k. \tag{2.3}$$

Where d is the acquired observation vectors $(d_1, d_2, \ldots, d_N)^T$, $\mathbf{G}$ is an $\mathbf{N} \times \mathbf{M}$ matrix (the model has dimension $\mathbf{M}$ but only $\mathbf{N}$ vectors) since $\mathbf{N} < \mathbf{M}$, and k is the $\mathbf{M}$'s values vector on 2.3. To solve the inversion problem, we must understand that it is an optimization problem, where we must construct an objective function to be minimized to produce an interpretable model according to equation (2.3).

In conclusion to solve an inverse problem, we must find a function out of a limited number of data, thus it is crucial to address fundamental problems regarding non-uniqueness and the misfit. We must define a misfit function ϕ_d and a model norm ϕ_m and minimize:

$$\phi_(m) = \phi_d + \beta\phi_m. \tag{2.4}$$

The misfit function ϕ_d is considered to be the "noise", it represents the relationship between the observed data and the predicted data. Therefore, we can say that

$$d^{obs} = F[m] + \eta + \delta. \tag{2.5}$$

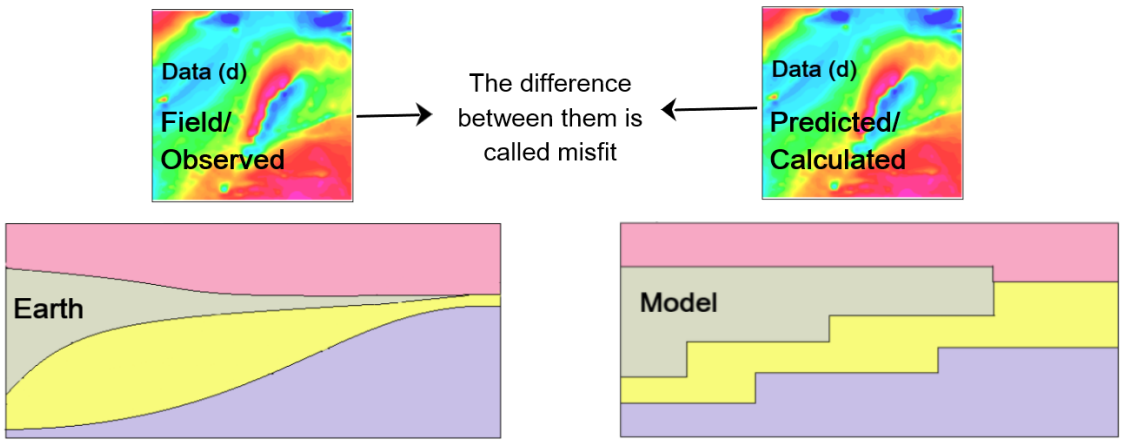

Figura 2.5: Measure of the difference between the observed data and the predicted data, also known as misfit.

Where η is related to measurements errors and δ is the actual difference between what is observed on earth and the mathematical response obtained (Figure 2.5).

But these terms are often not known, so the general rule is to presume that the error associated with the data is Gaussian, and that the standard deviation of the j'th datum is ε_j. The misfit is given by:

$$\phi_d = \sum_{j=1}^{N} \left(\frac{d^{obs} - F[m]}{\varepsilon_j} \right)^2 = \| W_d(d^{obs} - F[m] \|^2 . \tag{2.6}$$

Where $W_d = diag(\frac{1}{\varepsilon})$. With this we want to find a model that will effectively fits the data with some tolerable noise. The other term of the equation 2.4, that we are trying to minimize, is ϕ_m the model norm. We need to find a norm that will correctly recover the easiest model to interpret. Our intention is to obtain a solution that is close to a background value, has the slightest amount of noise, and please other prior information about the model. We define the model objective function as:

$$\begin{aligned}\phi_m(m) &= \alpha_s \int_v W_s\{w(z)[m(r)-m_0]\}^2 dv \\ &+ \alpha_x \int_v W_x\{dw(z)\left[\frac{m(r)-m_0}{dx}\right]\}^2 dv \\ &+ \alpha_y \int_v W_y\{dw(z)\left[\frac{m(r)-m_0}{dy}\right]\}^2 dv \\ &+ \alpha_z \int_v W_z\{dw(z)\left[\frac{m(r)-m_0}{dz}\right]\}^2 dv \end{aligned} \tag{2.7}$$

Where m_0 is the reference model, $w(z)$ is a depth weighting function; W_s, W_x, W_y and, W_z are spatially dependent weighting functions; and $\alpha_s, \alpha_x, alpha_y$ and, α_z are components coefficients. So, equation 2.7 allows us to construct different models depending on the assigned values for the variables. After adjusting these values, other information can be added to the model, such as from previous knowledge from the survey or from qualitative and quantitative interpretations made related to the susceptibility.

And finally, the β term from equation 2.4, also known as the the regularization parameter, ranging $0 < \beta < \infty$. It is intrinsic to the relationship between ϕ_d and ϕ_m. If β is too small, the function minimized will contain only the misfit ϕ_d. However, if β is too large, the recovered model will have the misfit too large. Choosing β based on the expected data misfit is known as the discrepancy principle (Parker, 1994).

2.4.4 The regularization parameter and the *L*-curve criteria

Estimate the regularization parameter is key to achieve the correct level of data misfit. We use the L-curve criterion to determine β directly from the analysis of the Tikhonov curve. The use of the L-curve for this type of inverse problems was first introduced by Lawson and Hanson (1974) and has been advocated by Hansen (1998).

To Exemplify, Figure 2.6 shows a typical Tikhonov curve. Region A of the curve is where $\beta \to \infty$, the misfit will be reduced and no large amount of structure will be added to the model. It means we are fitting the long wavelength structure in the data, that will better represent the physical model. In region B, $\beta \to 0$ so we are fitting high frequency components of noise in the data. The misfit does not increase despite the large amount of structure added to the model. These two regions are connected by a sharp corner between them, and that behavior is described as an L-curve.

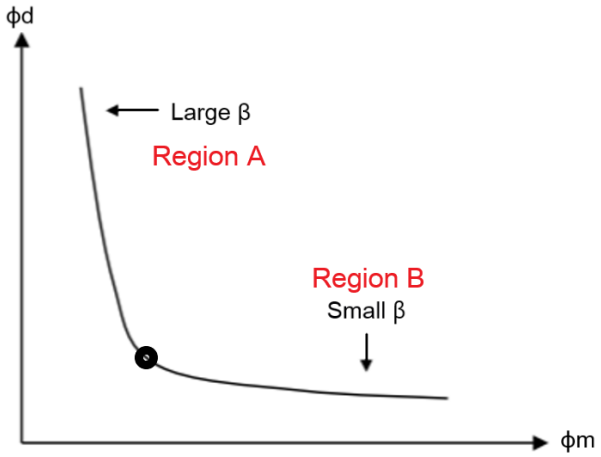

Figura 2.6: Typical Tikhonov curve. Through the L-curve criterion we determine the optimun "beta" directly from the sharp corner.

Hansen (1998) suggests that an optimum value for β corresponds to the inflexion of the curve. In a ϕ_d and ϕ_m plot this corner point can be evaluated numerically. Therefore, the model associated with the L-curvature must be the most fitting one.

2.4.5 Interpreting and understanding the inversion process

After we choose the appropriated parameters, we then preform the inversion. The result will be considered satisfactory when it is possible to make a correlation between the inversion model generated and the known geology. What really matters is the capability to perform an accurate interpretation, mainly due to the comprehension of the geological structure and expected magnetic susceptibility. If the inversion result is not satisfactory, we must find the source of the problem, calibrate the parameters and perform the inversion again, so that the process finally becomes less automated and more intuitive. The inversion process is not trivial and quite demanding in experience and knowledge, and the outcome will depend not only on the data processing but also it will depend on the interpretation of the preferred model. Figure 2.7 shows a fluxogram of the main inversion processes described in this section.

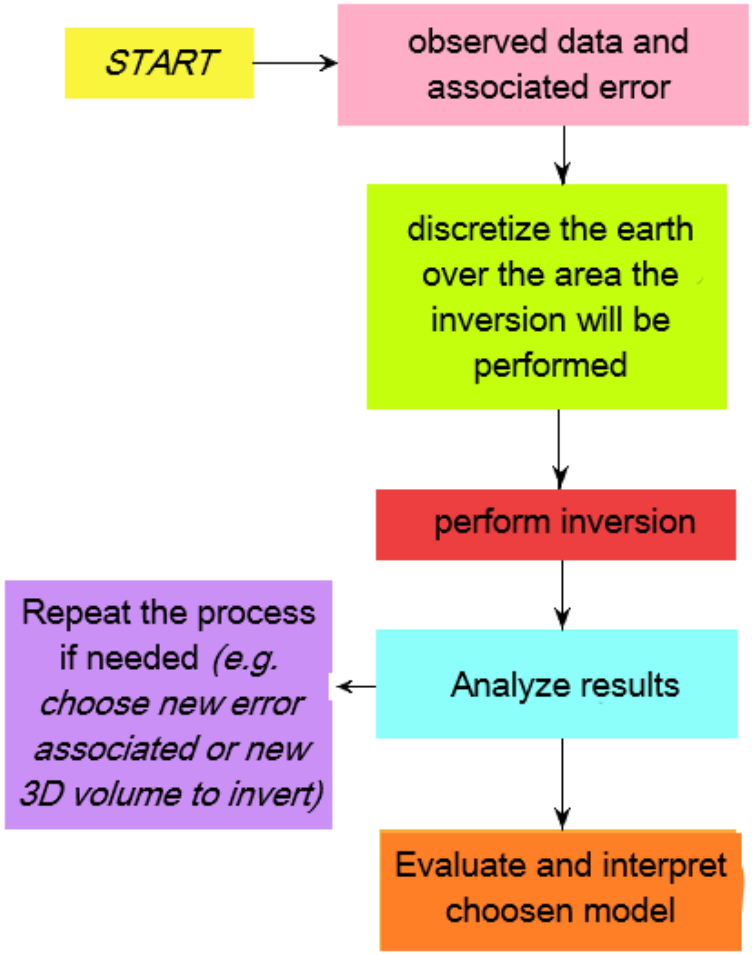

Figura 2.7: Inversion process fluxogram.

CHAPTER 3

3D characterization of the magnetic response of the Aimorés Intrusive Complex (Brazil): comparison with impact structures

This chapter presents the manuscript produced as a result of two years of research during the Master's program. It contains the methodology, results, discussion, and interpretations.

3.1 Abstract

The Aimorés Intrusive Complex (AIC), located in the Araçuaí Belt (Brazil), has been characterized for many years as the Aimorés Impact Crater due to its topographic features. The ellipsoidal to circular morphology, with an approximate diameter of 10 km, and the ring-shaped edges are easily recognized on satellite images. However, detailed geological mapping shows that its morphology is associated with a zoned igneous body, that was intruded during the post-collisional events related to the Araçuaí orogen. The intrusion is comprised of granitic to charnockitic rocks covered by quaternary lateritic deposits.

Although the Araçuaí Belt is well known and well-studied in terms of geochemistry and petrography, the understanding of the geophysics remains poorly understood. This study aims to characterize the AIC in 3D, understand the geometry of its lithological

zones, and compare its geophysical signature with those from impact craters. Through the integration of geological mapping and petrography, we propose a methodology for defining the susceptibility bound for constrained magnetic data inversions. The inversion results show a low susceptibility response at the central part of the AIC whereas higher values are identified in the post-collisional zoned igneous rocks in a semi-circular anomaly. These results are distinct, since higher values typically originate on the central-uplift of proved impact craters. We show that different structures can display similar characteristics on the surface while having different geometries in the subsurface.

3.2 Introduction

Located in the Araçuaí Belt (Brazil), the Aimorés structure has a crateriform expression, with a geomorphological expression suggestive of an impact feature as seen in Figure 3.1, as it presents features such as a circular pattern, raised arched edges and depressed central part, elliptical contour, centrifugal drainage and, semi-arched blocks facing the inside of the structure (Hachiro and Fernandez, 2004). These are some of the characteristics that contributes to the region being locally recognized as the "Aimorés crater". Also the structure has been listed as a possible impact structure in Brazil in the Expert Database on Earth Impact Structures (EDEIS). Although there are morphological evidences, more data is needed to classify it as an impact structure.

The major geological features of impact structures such as: circular forms, massive occurrence of igneous rocks, fracturing on the target rocks, circular patterns of deformation, and circular geophysical anomalies, are not exclusive features of these structures. The effective identification of such impact craters is based on a set of distinctive shock-metamorphic effects that are often expressed as the deformation in quartz grains, the formation of shatter cones, and the alteration in the local metamorphic grade, which are the unique products of impact-produced shock waves (French, 1968a; French and Short, 1968; French, 1998; Koeberl, 1997, 2002; Langenhorst, 2002).

The Araçuaí orogen, located in southeast Brazil, is a confined terrain surrounded by cratonic landmasses (Alkmim *et al.*, 2006, 2017; Pedrosa-Soares *et al.*, 2001, 2008, 2011a). It records an extensive granite production, revealing a correlation between the type of magmatism and the correspondent tectonic stage of the orogen (Chappel and White, 1974, 2001). Within the granitic rocks, it is possible to distinguish petrologic signatures related to each tectonic stage: pre-collisional, collisional, and post-collisional.

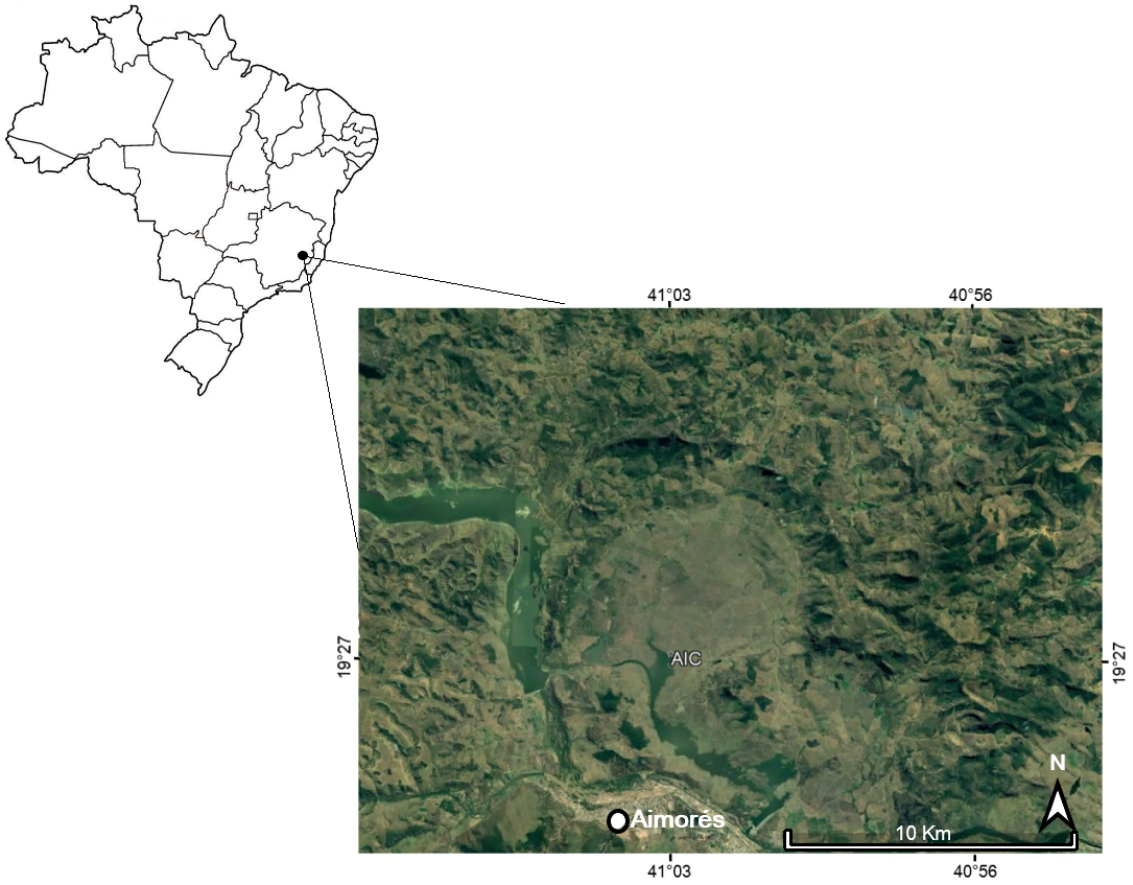

Figura 3.1: Satellite image of the Aimorés Complex (AIC). It is named after the city of Aimorés, south of the area.

Source: Image from Google Earth - 2021 Maxar Technology.

The orogen is subdivided into five granitoid supersuites named G1, G2, G3, G4, and G5, each of them corresponding to a geotectonic setting (Wiedemann, 1986, 1993; Ludka *et al.*, 1998; Pedrosa-Soares *et al.*, 2011a; Ludka *et al.*, 2000; S.Medeiros *et al.*, 2000; Medeiros *et al.*, 2001, 2003; Mendes *et al.*, 1997, 1999; Wiedemann *et al.*, 2002a). These were grouped into specific geotectonic stages (Pedrosa-Soares et al. 2008), namely: G1, pre-collisional (630-580Ma); G2, syn-collisional (585- 540Ma); G3 and G4, late-collisional to post-collisional (545-490Ma); and G5, post-collisional (530-480Ma). Although the supersuites are clustered into geotectonic stages, there is an overlapping transition from a tectonic context to another due to the unique magmatism complexity of the area (Pedrosa-Soares *et al.*, 2011a).

Detailed geological mapping of Aimorés region defined it as a zoned multistage

ring-like structure (Mello, 2011) and proved that it is one granitic intrusion of the G5 supersuite, a post-collisional plutonic body intruded into G2 sin-collisional rocks (Pedrosa-Soares *et al.*, 2011a). As the petrographical evidences required to prove an impact origin for the Aimorés structure haven't been identified yet, herein we refer to it as the Aimorés Intrusive Complex (AIC).

The structural, mineralogical, geophysical, and geochemical data analysis of the area is essential to explain the features of the Araçuaí orogen. The geological characteristics of the Araçuaí orogen have been extensively studied over the years, but the geophysical response of the different intrusions and its correspondent physical properties distribution in 3D remains underexplored. In this case, airborne geophysical data is a tool that enables the data acquisition of large domains where regional approaches are necessary. This technique is applied to comprehend structures in the subsurface as well as to interpret the surface relations among different lithologies.

The use of 3D modeling of magnetic potential field has become a useful tool as it provides information from the subsurface (Oldenburg, 2005). Over the past decades, the algorithms and computer calculations have been greatly improved leading to better-recovered models and better interpretations. Still, a great number of solutions can replicate the observed geophysical field data due to the non-uniqueness problem, and that can lead to a non realistic geological final model. That can be overcome when a priori knowledge is integrated in the modeling process (Fullagar *et al.*, 2008), which can assist the inversion algorithm to converge to a realistic model that better conveys the site geology. In this study, two sets of inversions were performed in order to achieve the optimal model, the first was an unconstrained inversion, whereas the second was an inversion constrained by lower and upper bounds.

Aiming to characterize the AIC geometry at depth, the inversion of airborne magnetic data was applied and 3D geology models of the subsurface were constructed. Through the inversion of magnetic data, we imaged the geometry of the AIC at depth and show the difference from an impact structure. We propose the use of petrographic data to define the upper susceptibility bound for the inversion. In order to integrate lithological information as a constraint to geophysical modeling. Also, we compare the results with the geophysical response of an impact structure to test if different geological structures could have similar geophysical responses.

The present manuscript will discuss the geological setting of the AIC, the methodology to perform the inversion and to perform the qualitative and quantitative analysis. We

then present the interpretations made over the susceptibility models generated. Finally, we compare the geophysical signature of impact structures with the one from the AIC.

3.3 Geological setting

The late Neoproterozoic to Cambrian Araçuaí orogen is located between the São Francisco craton and the Atlantic continental margin, in southeast Brazil, and has been intensely studied for the last forty years. Surrounded by significant cratonic masses, it contains impressive amounts of granitic rocks with distinct petrological signatures that mark the tectonic stages of the Orogen (Alkmim *et al.*, 2006, 2017; Pedrosa-Soares *et al.*, 1996, 2001, 2008, 2011a). Granite differentiation is closely related to magma rise during the pre-collisional stage and crustal thickening, especially during the collision and later stages due to the progressive rising of regional temperature as the metamorphic grade increases from west to east and from north to south across the orogen (Almeida *et al.*, 1978; Costa, 1989; Pedrosa-Soares *et al.*, 1996; Carvalho and Pereira, 1997). The magmatic pulses were subdivided into supersuites G1, G2, G3, G4, and G5 observed in Figure 3.2, according to its specific tectonic stages (Wiedemann, 1986, 1993; Ludka *et al.*, 1998; Pedrosa-Soares *et al.*, 2011a; Ludka *et al.*, 2000; S.Medeiros *et al.*, 2000; Medeiros *et al.*, 2001, 2003; Mendes *et al.*, 1997, 1999; Wiedemann *et al.*, 2002a).

The pre-collisional granitic rocks are associated with the lithosphere subduction and are well represented comprised by the granites type-I, meanwhile, whereas the collisional granites are linked with crustal thickening and correspond to the peraluminous type-S granites., and a At last, the post-collisional type-I granites are associated with a distensile tectonic setting (Pedrosa-Soares *et al.*, 2011a). This stage is represented by the G1 supersuite, which is mainly composed by tonalites and granodiorites with xenoliths of metasedimentary rocks and volcanic rocks from the Rio Doce Group. These bodies are mostly batholiths and stocks that often show a regional foliation and other deformation structures related with the further collision (Pedrosa-Soares and Noce, 2007). Some examples of volcanic rocks from this tectonic stage are pyroclastics tuffs, that occur with sparse volcanic rocks in the Palmital do Sul Formation; and tuffs from the Tumiritinga Formation, both interpreted as deposits of intra to anti-arch basins filled in the late-stage development of the magmatic arc. Also, there are the sedimentary contributions of the São Tomé Formation (Pedrosa-Soares and Noce, 2007).

The syn-collisional stage is characterized by a regional deformation and meta-

morphism, with extensive production of type-S granites (Nalini *et al.*, 2000; Pedrosa-Soares and Wiedemann-Leonardos, 2000; Pedrosa-Soares *et al.*, 2001; Campos *et al.*, 2004; Silva *et al.*, 2005). The regional metamorphism shows an increase in temperature, as the green-schist facies goes to granulite facies towards the nucleus of the orogen. Therefore, the metamorphism risesfrom west to east, and north to south (Almeida *et al.*, 1978; Pedrosa-Soares *et al.*, 2001; Trompette, 1994; Pedrosa-Soares and Wiedemann-Leonardos, 2000; Pinto *et al.*, 2001). This stage is related to the supersuite G2, which is essentially composed by peraluminous granites. These rocks occur in batholiths, tabular bodies and stocks that preserve the regional foliation, often mylonitic and parallel to the primary igneous flow (Nalini *et al.*, 2000; Celino *et al.*, 2000; Pedrosa-Soares and Wiedemann-Leonardos, 2000; Pedrosa-Soares *et al.*, 2001; Pedrosa-Soares and Castaneda, 2006; Pinto *et al.*, 2001; Campos *et al.*, 2004; Castaneda *et al.*, 2006). Rocks from the G3 supersuite are also identified as a product of the syn-collisional stage. Their representatives are essentially S-type granites and garnet-rich leucogranites (Pedrosa-Soares and Noce, 2007).

During the post-collisional tectonic stage, the gravitational collapse of the orogen produced an extensive plutonism (Pedrosa-Soares and Wiedemann-Leonardos, 2000; Pedrosa-Soares *et al.*, 2001; Campos *et al.*, 2004), represented by G4 and G5 supersuites. These are mainly intrusive plutons, non-foliated, , that originated the pegmatitic rocks in the district (Pedrosa-Soares *et al.*, 2001). The G4 supersuite often reveals rocks that are contemporaneous to the G3 rocks, and are considered as allochthonous bodies that were crystallized at higher crustal levels in relation to the G3 bodies (Pedrosa-Soares and Noce, 2007). The G5 supersuite, also post collisional, represents the plutonism characterized by I- and A-types, with predominant charnockitic and granitic compositions. There are also evidences of magma mingling and mixing, as well as the igneous flow direction. The major bodies are large batholiths of biotite-rich granite or pegmatitic charnockite (Pedrosa-Soares and Noce, 2007).

The AIC, object of this study, is one of the intrusions of the G5 suite, classified as a post-collisional plutonic body intruded into G2 sin-collisional rocks ((Pedrosa-Soares *et al.*, 2011a). There is a wide range of G5 bodies with different characteristics exposed along the Araçuaí orogen that occur as suites, batholiths, complex zoned plutons, sills, and dykes. Some exemples are the Aimorés, Caladão, Cotaxé, Guaratinga, Lagoa Preta, Lajinha, Medina, Padre Paraíso, Pedra Azul, Pedra do Elefante, Rubim, Santa Angélica, Salomão, Santo Antônio do Jacinto, and Várzea Alegre bodies (e.g. Silva *et al.* (1987); Wiedemann (1993); Pinto *et al.* (2001); Wiedemann *et al.* (1995, 2002b); Celino *et al.* (2000); Pedrosa-Soares and Wiedemann-Leonardos (2000); Campos *et al.*

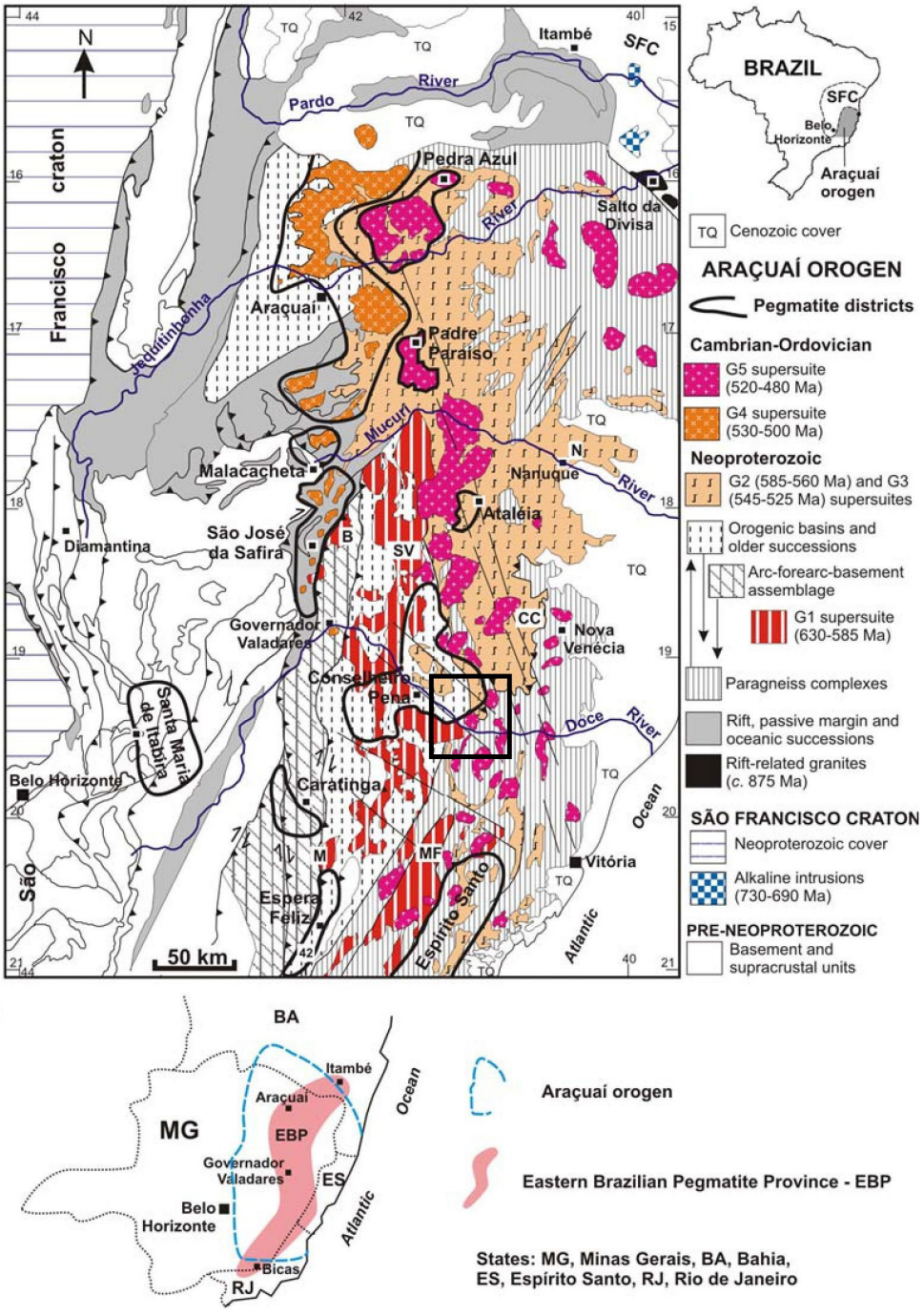

Figura 3.2: Simplified geological map of the Araçuaí orogen and adjacent cratonic region, (in Pedrosa-Soares *et al.* (2011a)). The black square shows the expanded study area. SFC = São Francisco craton. B = Brasilândia; CC = Carlos Chagas; M = Manhuaçu; MF = Muniz Freire; N = Nanuque; SV = São Vitor

Source: Pedrosa-Soares *et al.* (2011a).

(2004); Castaneda *et al.* (2006); Pedrosa-Soares and Castaneda (2006); Queiroga and Pedrosa-Soares (2009)). This supersuite commonly reveals evidence of magma mingling and mixing, observed due to the well-defined crystal orientations produced by igneous flow. However, due to the high erosion rates, levels of mafic cores are often absent. The G5 supersuite reveals post-collisional signatures, with calc-alkaline to alkaline granites that show high-K and high-Fe, recognized as I- to A2- types (Fernandes, 1991; Faria, 1997; Achtschin, 1999; Celino *et al.*, 2000; Whittington *et al.*, 2001; Pinto *et al.*, 2001; Sampaio and Martins, 2004; Pinto, 2008). These intrusions usually form inversely-zoned, balloon-shaped plutons composed of granitic-charnockitic rocks (Campos *et al.*, 2004), which is the case of the AIC.

The main units that occur in the study area are shown in Figure 3.3. The rocks from Paraíba do Sul complex have the highest metamorphic grades within the Araçuaí orogen, and consist of kinzigites; biotite gneiss with garnet, silimanite, cordierite in varying amounts, interspersed with gneisses rich in graphite; calcium silicate quartzites; and granulites (Pedros-Soares *et al.*, 1996).

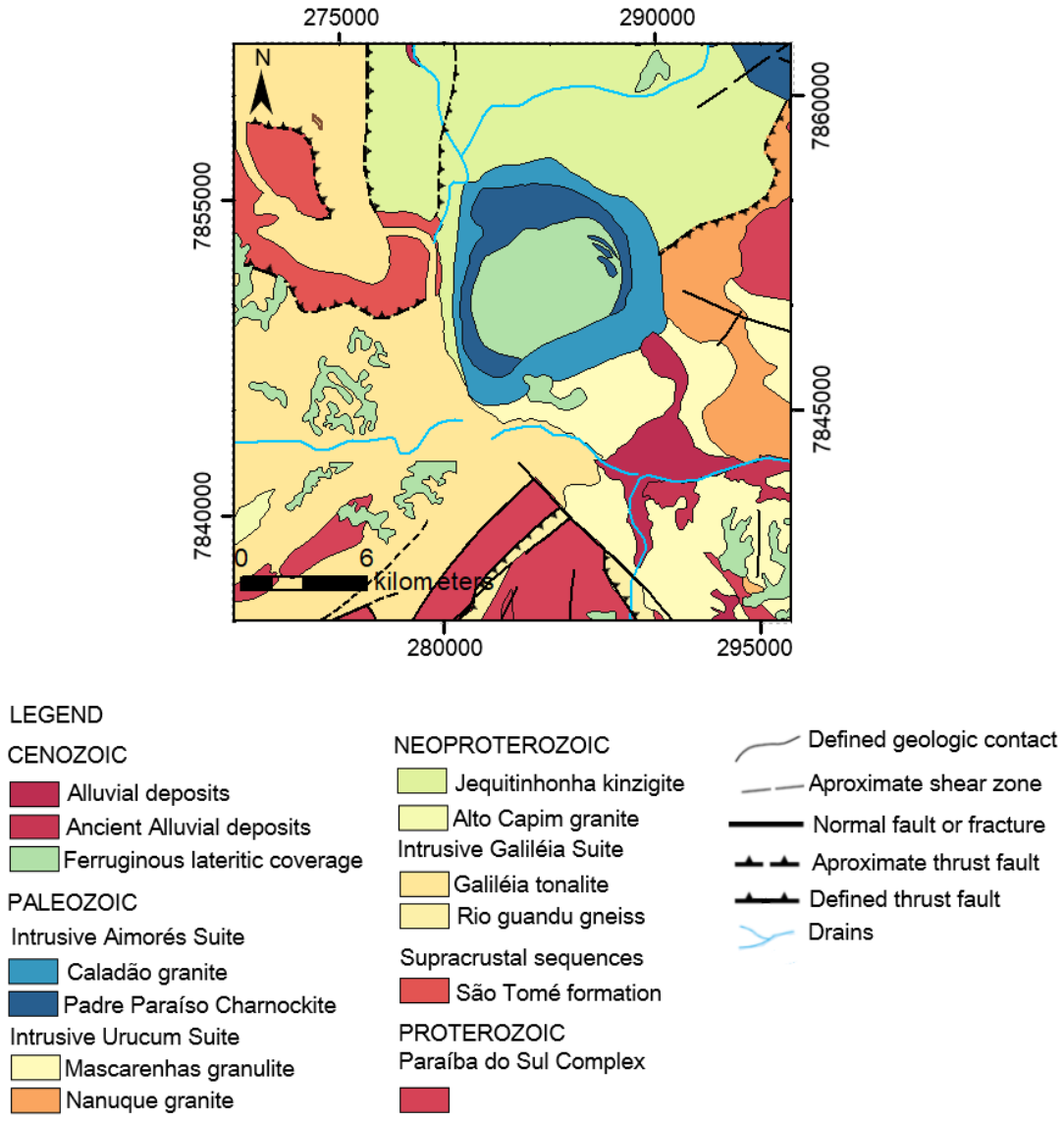

Figura 3.3: Simplified geologic map of Aimorés Complex.

Fonte: adaptado de CPRM (2010).

The São Tomé Formation is comprised by three units. The Unit One is composed mainly by quartzites; Unit Two by shales and quartzites; and Unit Three by shales and subordinate calcisilicatic rocks. The Unit Three is the only occurring unit in the area, consisting mainly of shales and gneisses. The shales are typically rich in plagioclase, quartz, muscovite, and biotite, with garnet, staurolite, and tourmaline occurring occasionally. The transition from schists to gneiss occurs gradually and is marked by the appearance

of sillimanite and kyanite (Pinto *et al.*, 1997).

The intrusive Galiléia Suite occurs as rocks that are often metaluminous to locally peraluminous, corresponding to I-type granites, with recurrent hornblende, allanite and titanite. These rocks are classified as sin-collisional granitoids (Pinto *et al.*, 1997). The Jequitinhonha kinzigite rocks are often weathered, displaying compositional bands that alternate between biotite-rich bands with feldspatic-quartz bands. The presence of cordierite and sillimanite are frequent (Pinto *et al.*, 1997).

The rocks from the Urucum intrusive suite are mainly S-type granites, from which mineralized pegmatite bodies occur (Pinto *et al.*, 1997). According to Nalini (1997), these granites are enriched in Na2O and depleted in MgO and CaO. Finally, the Aimorés intrusive suite comprehends two main units: the Caladão granite and the Padre Paraíso charnockite (Projeto Leste - CPRM, 2000). These rocks are rich in feldspar, quartz, biotite, apatite, hornblende, garnet, opaques minerals (magnetite and ilmenite), and secondary minerals (Pinto *et al.*, 1997).

The AIC is a ring-like, inversely-zoned structure, composed of basic to intermediate rocks such as tonalities, monzodiorites, quartz-monzodiorites, and granodiorites on its core. Towards the border, the rocks become progressively more acid (Mello, 2011). The main mineralogy recognized in these rocks is formed by amphibole, biotite, pyroxene, zircon and apatite grains (Mello, 2011). In the thin sections shown in Figure 3.4, there are two grains of an opaque mineral that could be magnetite or ilmenite according to Mello (2011). The mineralogy is basically the same in the Caladão granite and the Padre Paraíso charnockite, except for the presence of hypersthene and higher magnetite content in the Padre Paraíso charnockite. This is interpreted as a high-temperature residuum preserved in the function of the rapid rise of the body (Carvalho and Pereira, 1997a.). The AIC (Figure 4) is hosted by sin-collisional G2 rocks.

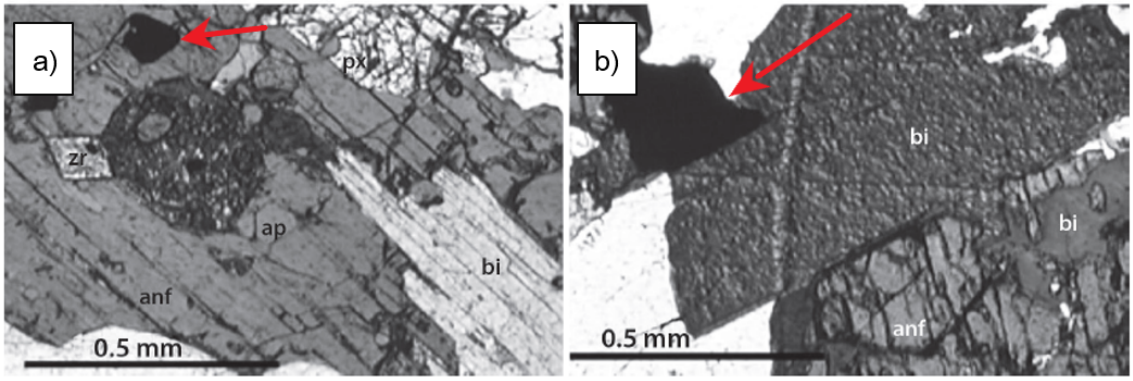

Figura 3.4: Microphotography of a charnockite sample of the AIC showing a) amphibole, biotite, pyroxene, zircon and apatite, and b) large crystal of biotite and amphibole. The opaque grains indicated by the red arrow could be magnetite or ilmenite.

Source: adapted from Mello (2011).

3.4 Geophysical data and inversion method

The airbone magnetic data used in this study was acquired from September 2009 to January 2010 with flight direction N-S and 500 m of line-spacing. The data were corrected for the International Geomagnetic Reference Field (IGRF) and diurnal variation in order to generate the Total magnetic intensity map (TMI). The magnetic field inclination is -35.7^o, the declination is -22.9^o, and field strength is 23,789 nT. The data were interpolated using the minimum curvature method. The gridding cell size used was $\frac{1}{4}$ of the larger flight line spacing (125 m). Then, a matched bandpass filtering was applied to separate the components of the wavelength spectrum produced by magnetic sources at different depths. When the short-wavelength components are removed, artifacts are eliminated from the flight line direction and the ambient noises are neutralized, therefore improving the data quality (Figures 3.5 and 3.6).

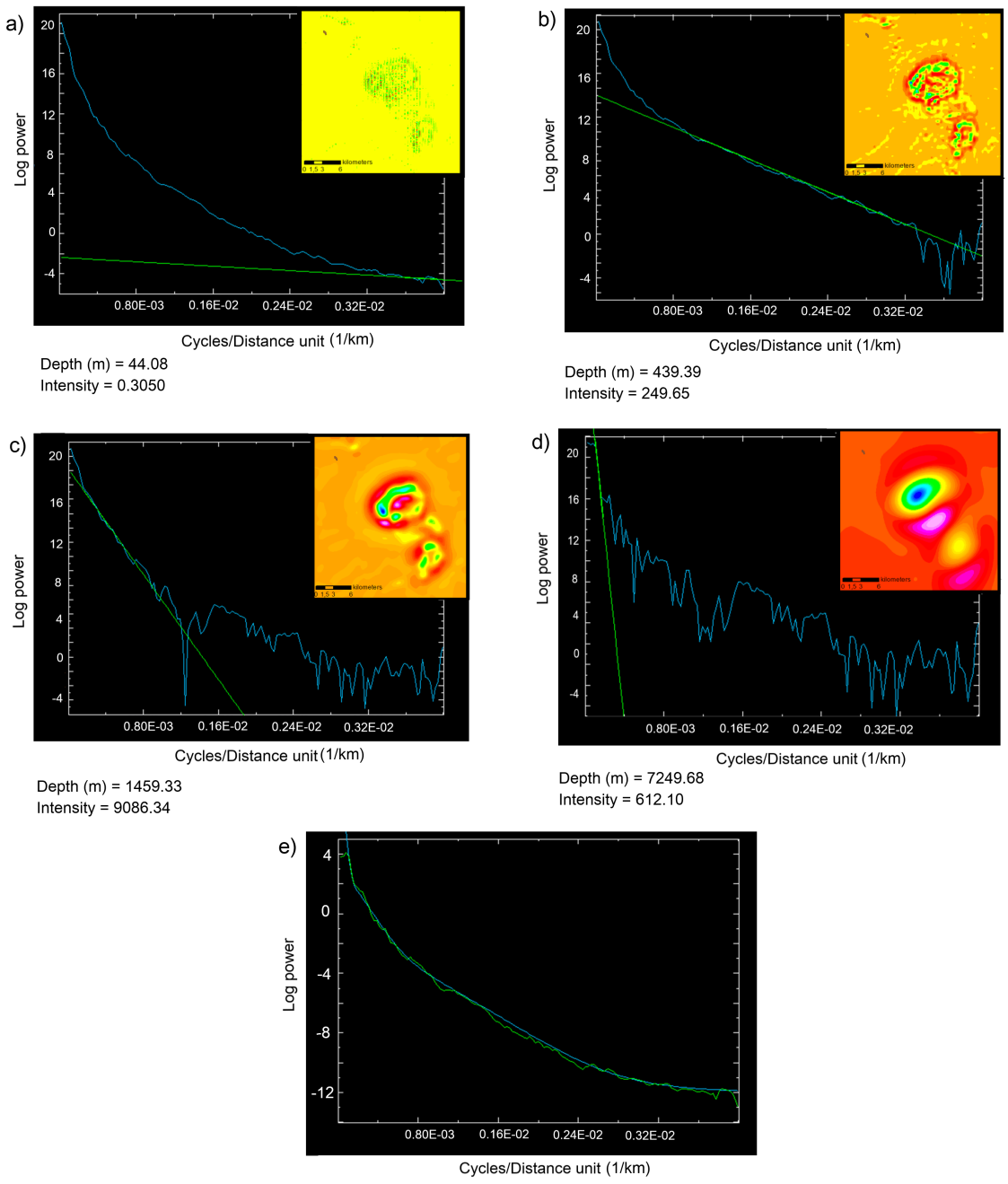

Figura 3.5: Result of the matched filtering in the study area showing the TMI image and power spectrum of a) the short wavelength, b) the intermediate wavelength I, c) the intermediate wavelength II, d) the long-wavelength, and e) the data power spectrum with the the bandpass modeled spectrum.

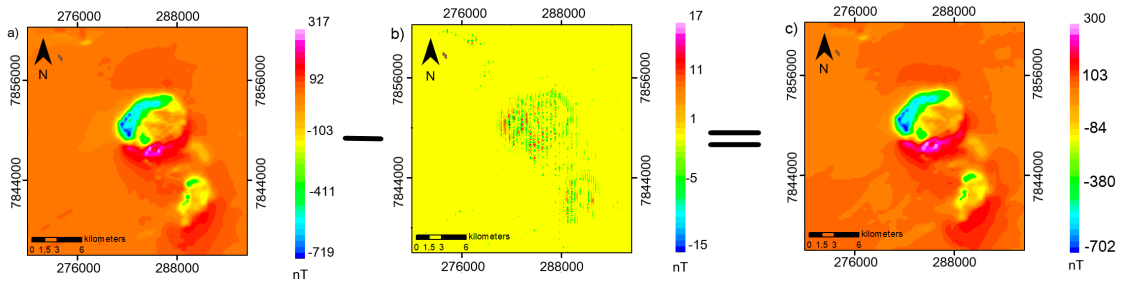

Figura 3.6: a) Image of the TMI over the AIC , b) the short wavelength part of the signal, and c) the residual TMI.

The total magnetic intensity (TMI) and the corresponding total gradient (Figure 3.7) show two main magnetic anomalies. Anomaly 1 , ranging from -10 nT to 300 nT, is associated with the AIC and shows a circular magnetic high associated with Padre Paraíso charnockite and in the center a magnetic low associated with superficial eluvial deposit over the Caladão granite. Anomaly 2, ranging from 20 nT to 200 nT, is associated with the Mascarenhas granulite, another G5 intrusion with similar response to AIC, i.e., magnetic ring with a low magnetic response in the center.

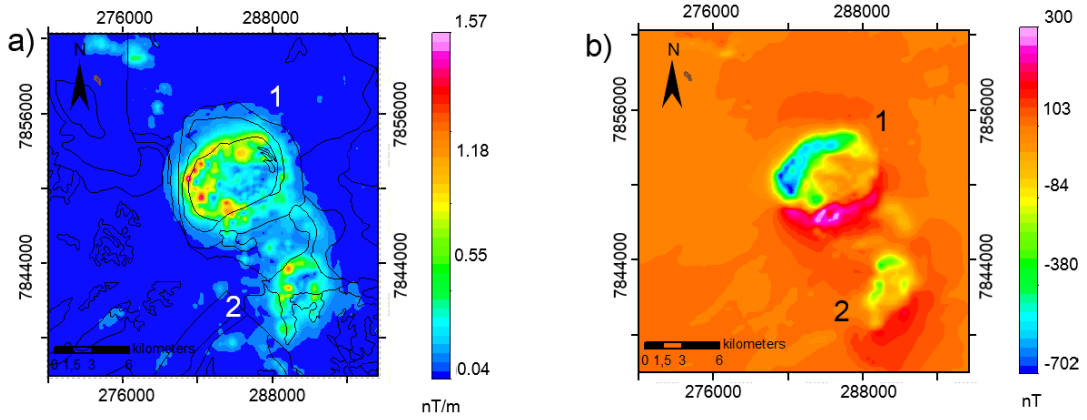

Figura 3.7: a) Total Gradient image overlain by the lithology contacts, and b) TMI image of the Aimorés complex.

Four main domains, subdivided into zones, were observed and delineated as shown in Figure 3.8. Domain 1 is characterized by low magnetic values and represents the majority of the host rocks in the Aimorés Complex. This domain consists of three zones, namely 1A, 1B, and 1C. Zone 1A displays the lowest magnetic responses, from 0.04 nT

to 0.13 nT. It is represented mainly by the Jequitinhonha gnaisse-kinzigitic complex, the Intrusive Galiléia suite, and other smaller bodies also from Supersuite G2, around the intrusive complex of Aimorés. In the southeast portion, the Zone 1B occurs over the Mascarenhas granulite and Nanuque granite, both from the Urucum intrusive suite and also over the same rock formations of Zone 1A. However, the magnetic response is slightly higher, from 0.13 nT to 0.17 nT. At last, Zone 1C displays an increase response that ranges from 0.17 nT to 0.38 nT.

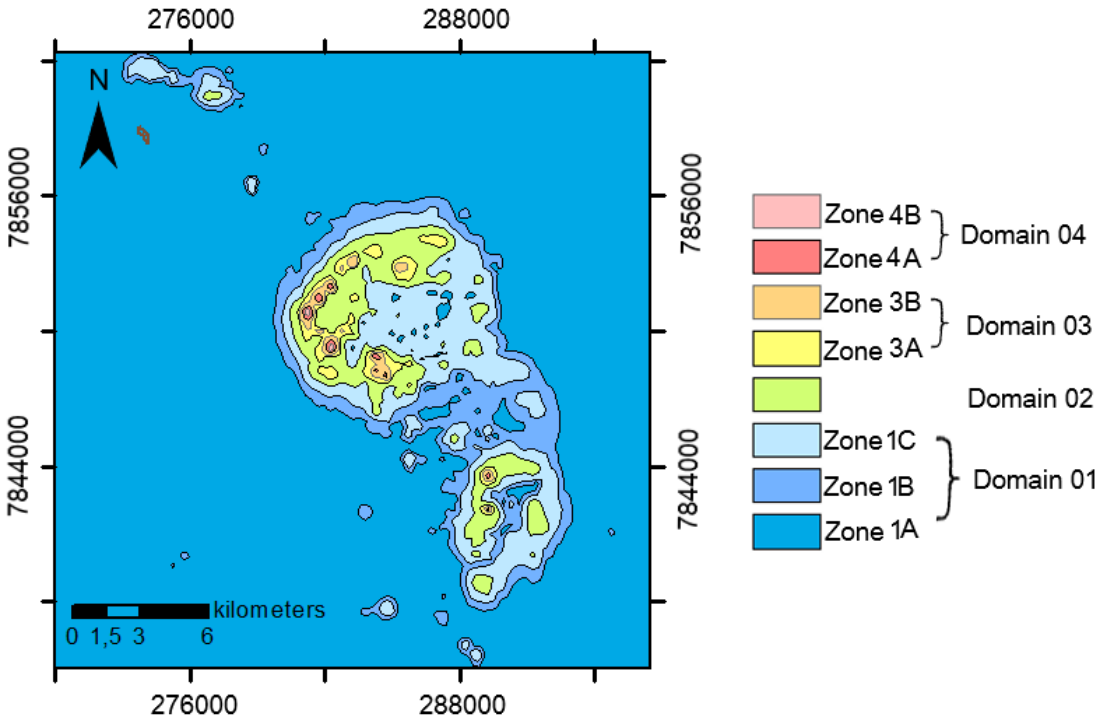

Figura 3.8: Magnetic domains based on the analysis of the total magnetic gradient of the study area.

Domain 2 has higher magnetic responses when compared to domain 1, from 0.38 nT to 0.72 nT. It displays low to intermediate values and occurs over alluvial and lateritic deposits that overlie the charnockitic portion of the Aimorés Complex, and the Mascarenhas granulite. Similarly Domain 3 is subdivided into two zones, both occurring over the same region of Domain 2, but differing in the intensity of the magnetic response. Zone 3A ranges from 0.72 nT to 0.85 nT, whhereas zone 3B goes from 0.89 nT to 1.15 nT.

Domain 4 is also subdivided into two zones and comprises the areas with the highest

magnetic response, in the south portion, Zone 4A occurs over the Mascarenhas granulite and ranges from 1.18 nT to 1.35 nT. Zone 4B occurs over the Padre Paraíso charnockite, partly covered by lateritic deposits, and ranges from 1.18 nT to 1.57 nT.

We observed that the charnockite was mapped in a semi-circular shape, but the analysis of the total gradient and the domain map shows that, in the east the magnetic content is much smaller than in the west. That analysis raises two questions: (1) Is there underneath the lateritic coverage a less magnetic portion of the charnockite? Or (2) Is it a new unmapped unit?

3.4.1 Magnetic inversion

In order to construct the inverted susceptibility model of the Aimorés structure in subsurface we used the 3D potential field inversion algorithm developed by Li and Oldenburg (1996). Intrinsic to the inversion of the potential data is the inherent nonuniqueness. According to Gauss's theorem, any magnetic field measured on the surface of the earth can be reproduced by an infinitesimally thin zone of magnetic dipoles in depth. Thus, there is not a depth resolution inherent in magnetic field data. Also, if one model exists and can reproduce according to the data, there must be other models that will reproduce the data to the same degree of accuracy (Li and Oldenburg, 1996).

To perform an inversion process, first the data, the error estimates, and information about the site must be known. The magnetic inversion is given by the linear equation:

$$\mathbf{d} = \mathbf{G}\mathbf{m} \tag{3.1}$$

Where $\mathbf{d}$ is the magnetic vector, $\mathbf{m}$ is the susceptibility vector of each one of the model cells and $\mathbf{G}$ is the matrix $N \times M$ (N is the number of data and M is the number of cells discretized). Then, an objective function needs to be calculated to produce the interpretable model by defining a misfit function ϕ_d a model norm ϕ_m and minimize ϕ:

$$\begin{aligned} & Min\ \phi(\mathbf{m}) = \phi_{\mathbf{d}} + \beta\phi_{\mathbf{m}} \\ \text{subject to} \quad & b_l \leq \mathbf{m} \leq b_u \end{aligned} \tag{3.2}$$

Where b_l and b_u are the upper and lower bounds of the model values (for the constrained inversion $b_l = 0$ and $b_u = 8 \times 10^3$), $\phi_{\mathbf{d}}$ is the data misfit function, $\phi_{\mathbf{m}}$ is the

model norm and, β is the regularization parameter that directly balances the importance of both other terms. This approach of choosing the β based upon the expected data misfit is called the discrepancy principle (Parker, 1994).

It is important to understand the error contained in geophysical measurements before proceeding with the method, or the final model could display artifacts. The error assigned was 2% of the absolute value of the measurements, corresponding to 20.87 nT. The Tikhonov curve was then constructed in order to identify the β that corresponds to the tradeoff that balances between a small enough misfit and the model norm. This was enabled by the use of different regularization parameters ranging in wide orders of magnitudes. After running several inversions with a range of β's, the L-curve criterion (Hansen, 1992) with the analysis of the smaller value of $\phi_{\mathbf{d}}$ associated was applied to select the appropriate β. Figure 3.9 shows a typical L-curve and the relation between the misfit and the model norm.

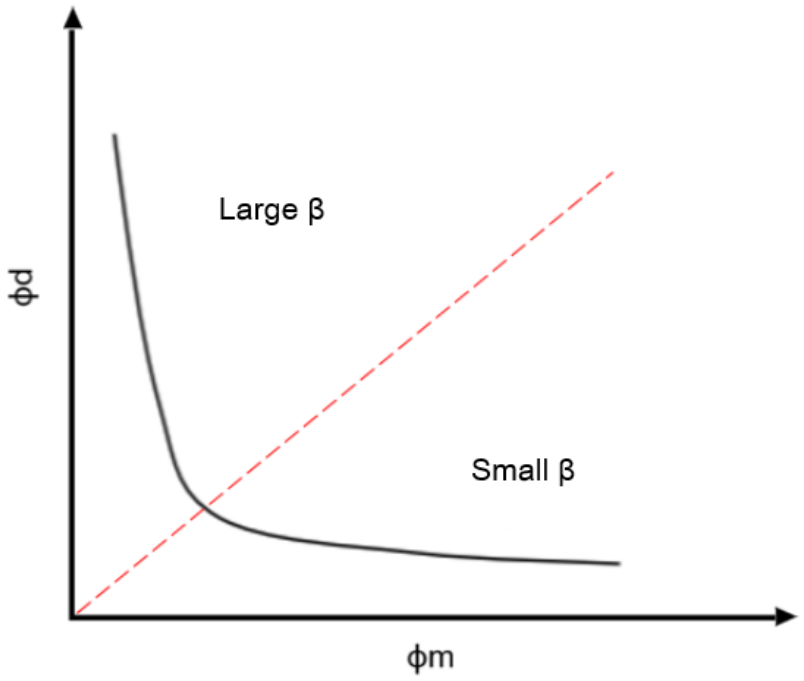

Figura 3.9: L-curve, the role of β in a $\phi_{\mathbf{d}}$ versus $\phi_{\mathbf{m}}$ graph. Large β corresponds to theunderfit zone, where the geological information is not incorporated. Small β corresponds to the overfit zone where a lot of artifacts that are not geological are incorporated.

In this study, two sets of inversions were performed in order to achieve the optimal

model, the first was an unconstrained inversion, whereas the second was an inversion constrained by lower and upper bounds for magnetic susceptibility.

The inversion was performed using a mesh with 46650 voxel cells and the mesh is composed of cubic cells of 125 × 125 × 125 m. Padding cells with increasing widths from the core region were used in depth and in north, south, west, and east directions to ensure the data would not suffer any distortion. The study area extends 27 km in the east-west direction, 29 km in the north-south direction, and 10 km in depth. After analyzing the residual images, the inverse solution from the "edge" of the L-curve was considered. However, as one model close to the edge has a smaller value of $\phi_{\mathbf{d}}$ associated, it was selected as the best solution. The L-curve and the residual map are shown in (Figures 3.10, 3.11,3.13, and 3.14).

As petrographical studies of the area have shown that the charnockite zone has 3% of magnetite (Mello, 2011). This data was incorporated as a constraint in the geophysical inversion. Using the relation between the content of magnetite and the magnetic susceptibility we estimated the upper bound for the magnetic inversions as seen in (Figure 3.12).

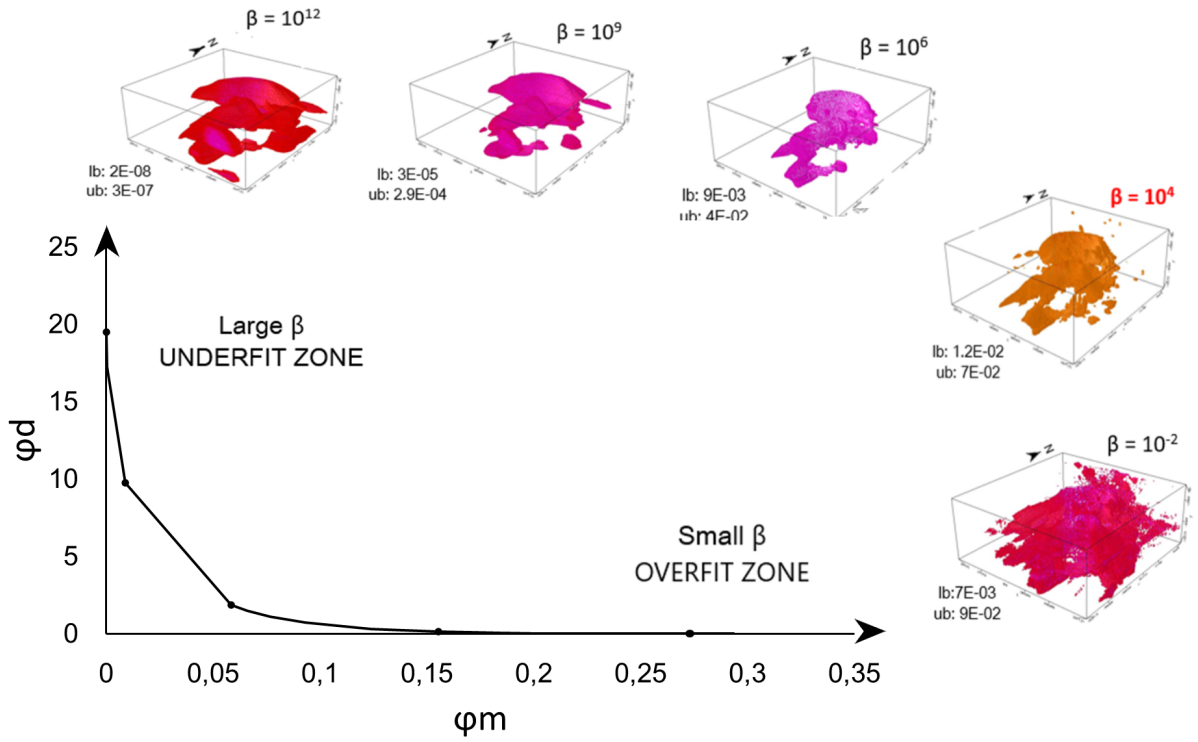

Figura 3.10: L-curve from the unconstrained inversion process. The best recovered model is the one with $\beta = 10000$.

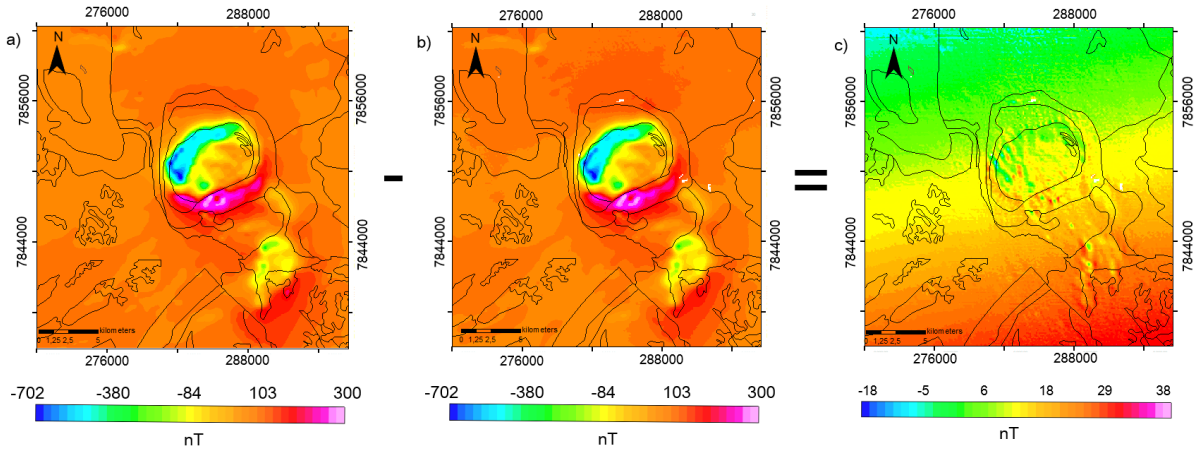

Figura 3.11: Residual image of the best recovered model of the unconstrained inversion. a) Observed TMI of the area b) Predicted TMI of the area. c) Residual image of the best recovered model.

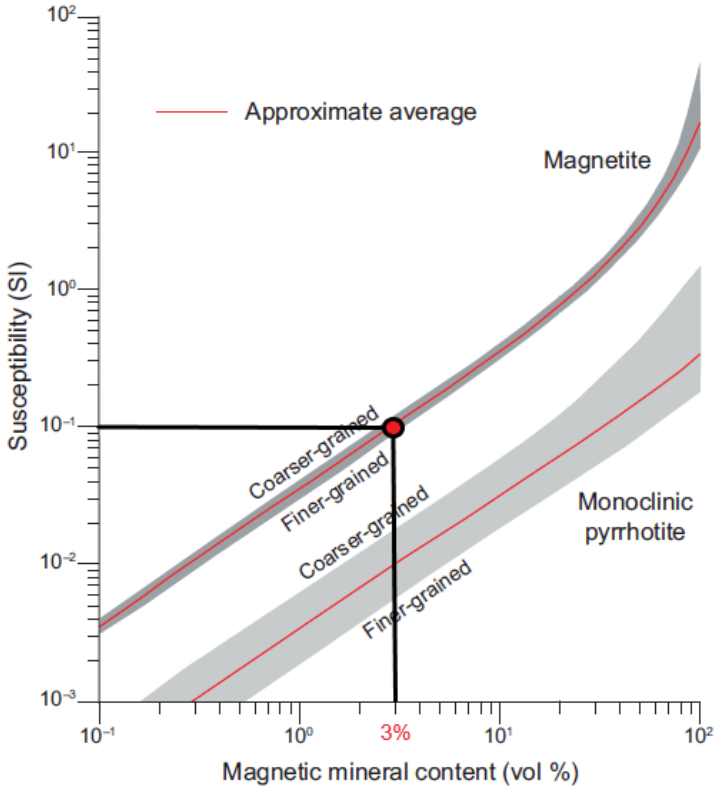

Figura 3.12: Graph of the magnetic susceptibility plotted *versus* the volumetric content of magnetite and pyrrhotite showing that the susceptibility corresponding to 3% of magnetite is 10-1 SI.

Source: adapted from Clark (1997) in Dentith and Mudge (2014).

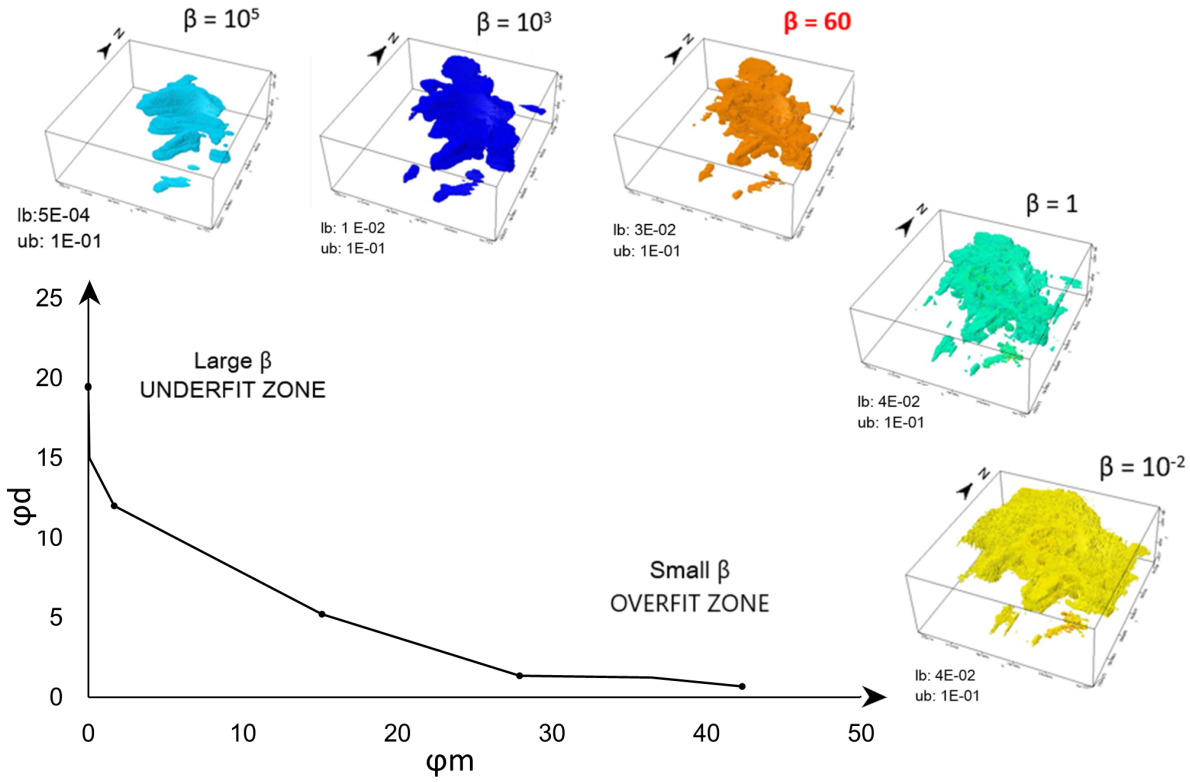

Figura 3.13: L-curve from the constrained inversion process. The best recovered model is the one with $\beta = 60$.

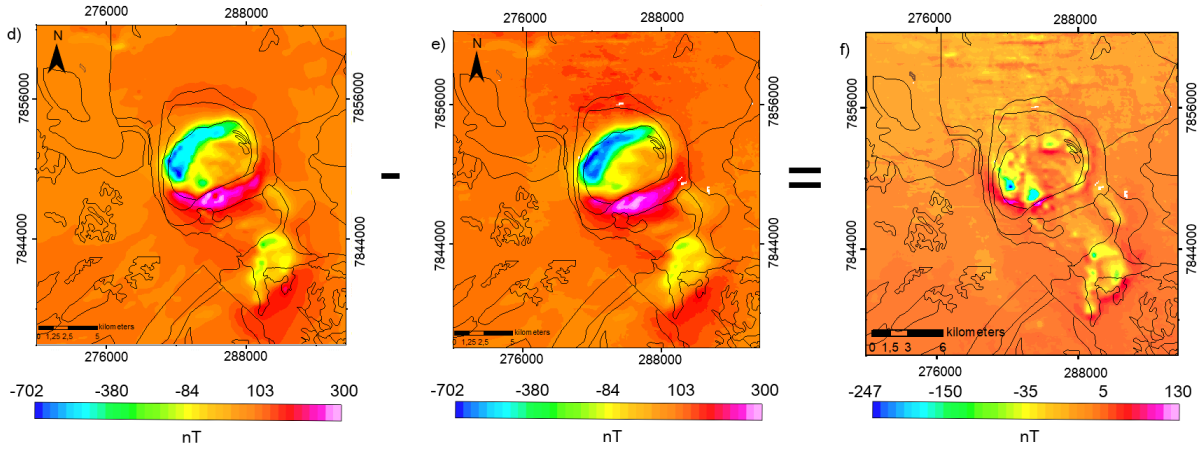

Figura 3.14: Residual image of the best recovered model of the constrained inversion. d) Observed TMI of the area e) Predicted TMI of the area. f) Residual image of the best recovered model.

3.5 Interpretation of the magnetic data and 3D susceptibility model

Inversion of magnetic susceptibility using the Voxi model of Oasis Montaj software resulted in a susceptibility contrast distribution. The recovered susceptibility model shows a contrast between the granitic rocks from the Supersuite G5 and G2 (Figures 3.15, 3.16, and 3.17). The low susceptibility area is associated with the G2 host rocks, which are peraluminous, calc-alkalic to sub-alkalic S-type granites of the pre to late-collisional stage. Three main bodies of high susceptibility are identified: Body A is associated with the AIC, Body B is deeper and have no expression on the surface, and Body C is associated with the Mascarenhas granulite.

Body A has a circular shape with the higher susceptibility values in its northwestern part. Within this area, there is a nucleus with the highest susceptibility values. This ring of high susceptibility corresponds to the Padre Paraíso charnockite unit. The magnetic ring is around a non-magnetic core region associated with the Caladão granite. The AIC is composed of metaluminous to slightly peraluminous I-type granitoids of the post-collisional stage.

Body B does not outcrop and is connected to A at depth (Figure 3.17), showing that the charnockite intrusion has a deep root and extends to the northwest of the AIC. Body C is located in the southeast of the AIC and is associated with the Mascarenhas granulite. This granulite is porphyritic and has a composition similar to the Padre Paraíso charnockite, but shows an incipient foliation. The 3D susceptibility distribution of the AIC does not show high values in the center, which is usually is expected in large impact structures.

3.5.1 Magnetic similarities and differences between Aimorés and impact structures

The AIC shows a low magnetic response in its center, which is typical of simple impact structures, that have small diameters. However, the diameter of the AIC circular topography is larger than the threshold for simple impact structures, and thus could only be a complex impact structure.

For comparison we analyzed Hawke (2004) work that compilated the geophysical signatures of Australia's meteorite impact structures. The Acraman crater, on the Gawler

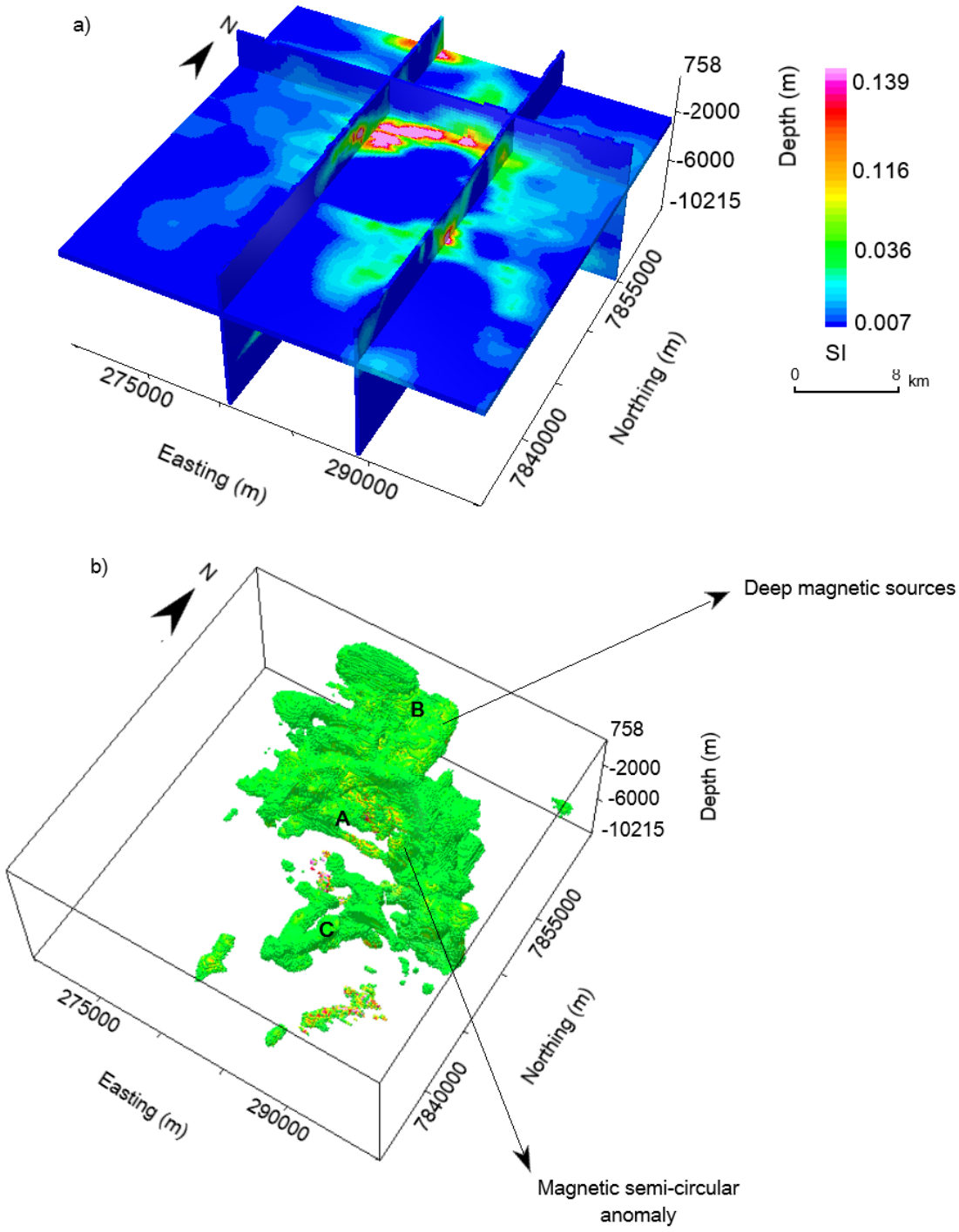

Figura 3.15: a) Recovered susceptibility model showing b) a vertical section at 288300 North and a depth slice at -2500 m, and a cutoff of 0.036 SI. A: corresponds to the AIC susceptibility recovered; B: corresponds to the deep root extending to North; C: corresponds to the Mascarenhas granulite susceptibility recovered.

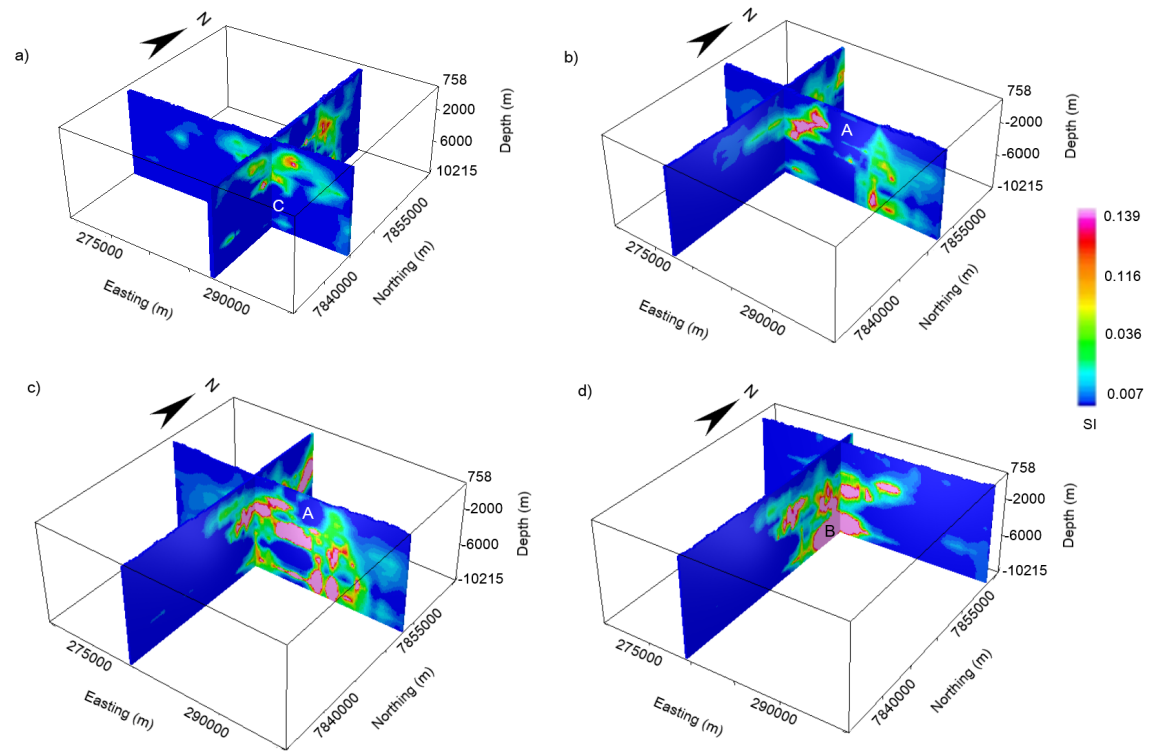

Figura 3.16: Vertical sections of the model a) Vertical section at 7844700 North. Body C corresponds to the Mascarenhas granulite b) Vertical section at 7852000 North. Body A corresponds to the AIC c) Vertical section at 78532000 North. Body A corresponds to the AIC. d) Vertical section at 78606000 North. Body B corresponds to the deep root extending to North.

Ranges of Australia, is an example of a complex structure formed in crystalline target rocks and its geophysical data suggest a single-peak uplift, defined by a circular zone of low magnetic intensity explained by the shock demagnetization of the target rocks by the impact. A strong magnetic response to the south coincides with the outcropping dacite. A small magnetic high located near the middle of the central uplift is observed in Figure 3.18-a, roughly with 5 km in diameter and has an amplitude of 800 nT (Hawke, 2004). Schmidt and Williams (1996) suggest that the anomaly was caused by a remanently magnetized source centered 1km below the surface level.

The Yallalie structure also located in Australia, is a shallow circular depression of about 13 km in diameter with a central uplift of 3.4 km diameter that occurs within Mesozoic sedimentary rocks of the Perth Basin. The magnetic response of this crater is quite remarkable, since it shows concentric circular magnetic anomalies centered in

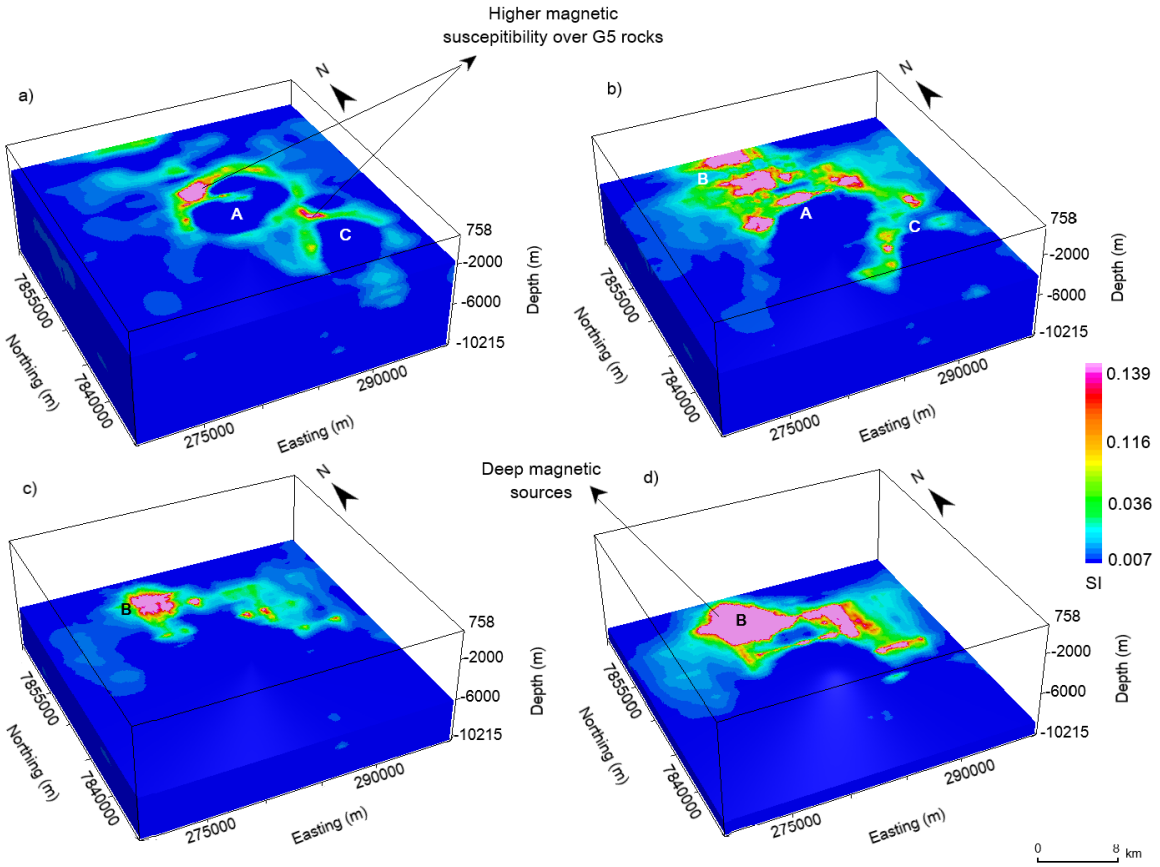

Figura 3.17: Depth slices of the recovered susceptibility model at a) -1800 m, b) -4200 m, c) -6200 m, and d) -9000 m.

a peak, a little bit off the center. According to Pilkington *et al.* (1996), this type of magnetic anomaly at the peak might be created by a local hydrothermal system driven by the heat generated by the impact, along with internal faults. Figure 3.18-b shows the geophysical response of the structure.

The Foelsche structure on the northern territory of Australia, is a 6.2 km diameter structure that can be observed from satellite images and geological mapping (Haines and Rawlings, 2002). It is demarked by a low magnetic circular anomaly of 5.5 km in diameter with a smaller concentric magnetic anomaly of 2.1 km which is interpreted as the central uplift (Figure 3.18-c). The magnetic unit is comprised by doleritic sills of the settlement creek volcanics, which are folded and tilted around the central uplift and the outer rim of the crater due to the impact (Hawke, 2004).

The small Wolf Creek Crater, located in the Kimberley Region of Western Australia,

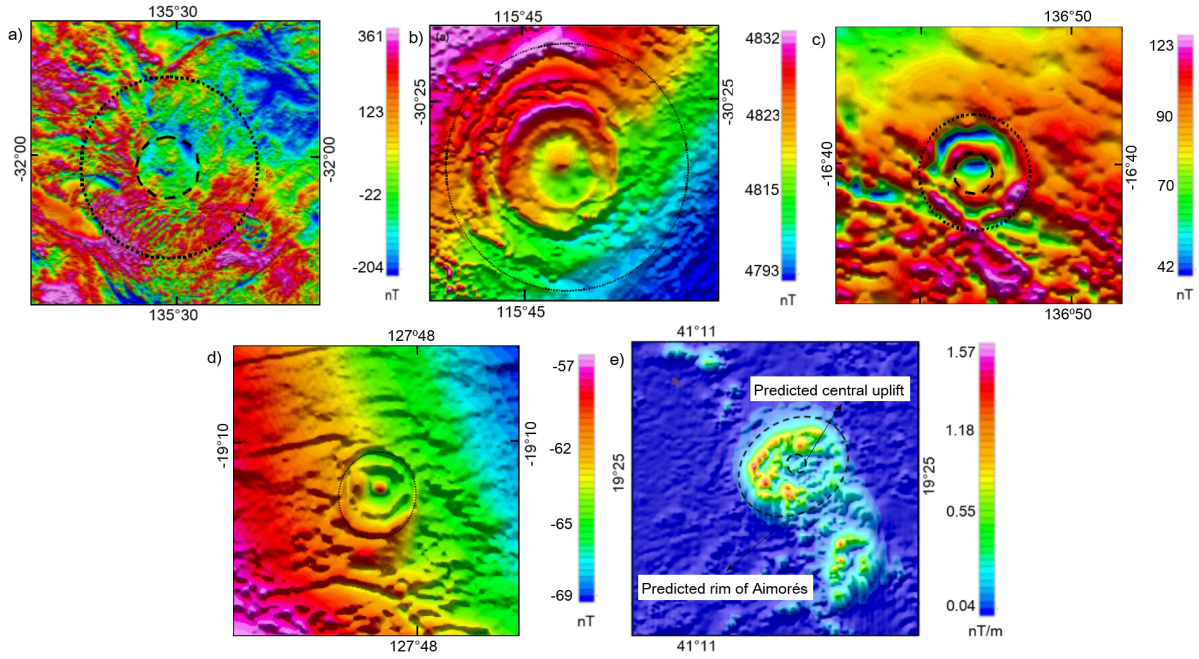

Figura 3.18: TMI of the Acraman structure. b) TMI of Yallalie structure. c) TMI of Foelsche structure. d) TMI of Wolf Creek structure and e) Total Gradient of Aimorés. The dashed line represents the central uplift of the craters, the dotted line represents the structural rim of each structure.

, has an average diameter of 880 m and was formed in sandstones of the Mesoproterozoic Birrindudu Basin (Blake *et al.*, 1977). Due to the quartzite target, the variation in the magnetic field over the crater is very subtle. The range of the TMI over the area is 12 nT, largely due to a W-SW linear magnetic regional trend of 2.5 nT/Km, that is coincident with longitudinal sand dunes that concentrate small portions of heavy minerals. In Figure 3.18-d, we see the circular anomaly, concentric around a single peak, correlate with the crater rim (Hawke, 2004).

In the study area, the AIC does not show a central uplift and an associated positive magnetic anomaly as shown in the total gradient image of the AIC (Figure 3.18-e).

3.6 Conclusion

The results show the importance of incorporating geological constraints into geophysical modeling, especially in ambiguous geological settings, in order to achieve more accurate geological interpretations. The proposed method, using the mineralogy recogni-

zed in petrographic thin sections for estimating the upper susceptibility bound of the geophysical inversions, allowed the construction of a model compatible with field data.

Despite the morphological expression of the AIC, its geophysical signature shows a magnetic susceptibility distribution that is not expected from an impact structure. The AIC has a low magnetic anomaly over its center and does not display the characteristic central magnetic peak of impact structures.

The interpretation of the 3D model also reveals a clear differentiation of G2 and G5 supersuites, according to the distinct magnetic responses.Thus, the characterization of these bodies through their magnetic response is a powerful tool to support the geologic mapping of the region, since the circular magnetic patterns from other bodies in the Araçuaí orogen could also be recognized. Given the geophysical analysis, it was observed that the Aimorés complex has three units in fact: external granite, semi-circular charnockite, and a third non-magnetic region under the lateritic coverage;

Furthermore, two main G5 igneous bodies that occur on the site were distinguished, as well as the positive anomalies associated with its borders and the low anomalies at the center. Finally, it was also possible to observe an anomaly in depth that has no superficial expression, and could be a topic for further research.

CHAPTER 4

Future works

4.1 Suggestions and advices for future research

The geophysical analysis in 2D and the magnetic inversion of the data of the AIC allowed us to interpret the 3D model and to identify the susceptibility response of the two main igneous intrusions of the G5 supersuite. However, future study is necessary to increase the knowledge of the area and corroborate with the discussion presented in Chapter 3. Therefore, further research might:

1. Perform detailed fieldwork and sampling campaigns
   - The analysis of rock samples is crucial to identify typical features of impact craters, one with a trained eye might be able to find evidences of the event in a more specific fieldwork campaign;
   - Also, the direct susceptibility measurement of the site's rocks will increase the accuracy of the constrain that limited the inversion result.
2. Acquisition and inversion of data from other geophysical methods

   The inversion of the magnetic susceptibility is one type of inversion possible to study the structure and recover interpretable models. There are other physical properties such as density, seismic velocity and electrical conductivity that, depending on the availability of the data or the possibility to acquire it trough a geophysical survey, would make the interpretations more robust.

3. Compare the geophysics of similar intrusions

   It is a known fact that the G5 intrusions are formed under the same geotectonic context, so it would be interesting to analyze the geophysical response of similar complexes to see the behavior in subsurface of each one of them.

References

Achtschin, A., 1999. Caracterização geológica, mineralógica e geoquímica dos pegmatitos do distrito de padre paraíso, minas gerais, e suas variedades de berilo. Ph.D. thesis, UFMG.

Alkmim, F., Kuchenbecker, M., Reis, H., Pedrosa-Soares, A., 2017. The araçuaí belt. In: São Francisco Craton, Eastern Brazil: Tectonic Genealogy of a Miniature Continent. Springer International Publishing, p. 255Ű276.

Alkmim, F., Marshak, S., Pedrosa-Soares, A., Peres, G., Cruz, S., Whittington, A., 2006. Kinematic evolution of the araçuaí Ű west congo orogen in brazil and africa: Nutcracker tectonics during the neoproterozoic assembly of gondwana. Precambrian Research 149, 43–63.

Almeida, F., Hasui, Y., Rodrigues, E., Yamamoto, J., 1978. A faixa de dobramentos araçuaí na região do rio pardo. Phd.

Blake, D., Passmore, V., Muhling, P., 1977. Bililliluna, western australia Ű 1:250000 geological series explanatory notes, se52-14. Bureau of mineral ressources, australia.

Campos, C. D., Mendes, J., Ludka, I., Medeiros, S., Moura, J., Wallfass, C., 2004. A review of the brasiliano magmatism in southern espírito santo, brazil, with emphasis on post-collisional magmatism . j. virtual explor 17, 1,39.

Carvalho, J., Pereira, L., 1997. Caracterização petrológica das rochas graníticas e charnockiticas da porção leste do estado de minas gerais baseada em dados petrográficos. In: SBG, Boletim 14. Simpósio de Geologia de Minas Gerais, p. 941Ű969.

Castaneda, C., Pedrosa-Soares, A., Belem, J., Gradim, D., Dias, P., Medeiros, S., Oliveira, L., 2006. Folha ecoporanga. Programa geologia do brasil, CPRM Ű Serviço Geológico do Brasil.

Celino, J., Botelho, N., Pimentel, M., 2000. Genesis of neoproterozoic granitoid magmatism in the eastern araçuaí fold belt, eastern brazil: field, geochemical and srŰnd isotopic evidence. Revista Brasileira de Geociencias 39 (30), 135–139.

Chappel, B., White, A., 1974. Two contrasting granite types. pacific geology (8), 173–174.

Chappel, B., White, A., 2001. Two contrasting granite types: 25 years later. (48), 489–499.

Clark, A., 1997. Magnetic petrophysics and magnetic petrology: aids to geological interpretation of magnetic surveys. AGSO Journal of Australian Geology and Geophysics (17), 83–104.

Clark, J., 2001. Magnetic survey data at meteoritic impact sites in north america, geomagn. serv. ca. Open File Rep, 83–5, 1–30.

Cobbing, J., 1996. Granites - an overview 19, 103–106.

Costa, A., 1989. Evolução petrológica para uma sequência de rochas metamórficas regionais do tipo baixa pressão, itinga, ne-mg. Revista Brasileira de Geociências (19), 440–448.

CPRM, 2010. Projeto leste, etapas 1 e 2. cprm-comig, belo horizonte, cdrom. Tech. rep., CPRM - COMIG.

Crósta, A., 2012. Semiautomated geologic mapping using self-organizing maps and airborne geophysics in the brazilian amazon. geophysics v, 17,24.

Dabizha, A., Fedynsky, V., 1975. The earthŠs Şstar woundsŤ and their diagnosis by geophysical methods, zamlya vselennaya 3, 56-64, 1975. Tech. rep.

Dentith, M., Mudge, S., 2014. Geophysics for the Mineral exploration Geoscientis. Cambridge University Press.

Dietz, R., 1969. Meteorite craters and astroblemes: New information. Meteoritics v, 269.

Faria, L., 1997. Controle e tipologia de mineralizações de grafita flake do nordeste de minas gerais e sul da bahia: uma abordagem regional. Ph.D. thesis, Inst. Geociências, Universidade Federal de Minas Gerais, Belo Horizonte, Brazil, MSc thesis, 102 p.

Fernandes, M., 1991. Geologia, petrografia e geoquímica de rochas granitoides da região de pedra azul, mg. Ph.D. thesis, Inst. Geociências, Universidade Federal do Rio de Janeiro, Brazil, MSc thesis, 191p.

French, B., 1968a. Shock metamorphism as a geological process. in: French, b.m.,short, n.m. (eds.), shock metamorphism of natural materials. Mono Book Corp, Baltimore, MD, 1Ű17.

French, B., 1998. Traces of catastrophe: a handbook of shock-metamorphic effects in terrestrial meteorite impact craters. Tech. rep., Lunar and Planetary Institute, Houston, TX, Contribution CB-954. 120 pp.

French, B., 2005. Stalking the wily shatter cone: a critical guide for impact-crater hunters. impacts in the field, vol. 2 (winter, 2005. Tech. rep.

French, B., Koeberl, C., 2010. The convincing identification of terrestrial meteorite impact structures: What works, what doesn't, and why. Earth-Science Reviews (98(1-2)), 123–170.

French, B., Short, N., 1968. Shock Metamorphism of Natural Materials. Mono BookCorp, Baltimore, MD.

Fullagar, P., Pears, G., McMonnies, B., 2008. Constrained inversion of geologic surfaces Ű pushing the boundaries. lead edge (tulsa, ok). 27:98Ű105. Tech. rep.

Grieve, R., 1991. Terrestrial impact: the record in the rocks. Meteoritics (26), 175,194.

Grieve, R., 1998. Extraterrestrial impacts on earth: the evidence and the consequences. in: Grady, m.m., hutchison, r., mccall, g.j.h., rtechreporty, d. (eds.), meteorites: Flux with time and impact effects. Geological Society, London, Special Publication vol. 140 (26), 105,131.

Grieve, R., Garvin, J., Coderre, J., Rupert, J., 2010. Test of a geometric model for the modification stage of simple impact craters development. Meteoritics (24), 83,88.

Hachiro, J., Fernandez, V. V., 2004. A estrutura oval de aimorés (mg): evidências morfo-estruturais e petrográficas de crateramento por impacto. in recursos minerais e desenvolvimento socioeconomico. Tech. rep., SBG.

Haines, P., Rawlings, D., 2002. The foelsche structure, northern territory, australia: an impact crater of probable neoproterozoic age. Meteoritics and Planetary Science (37), 269–280.

Hansen, C., 1998. Rank deficient and discrete ill posed problems: numerical aspects of linear inversion. Folha, Society for Industrial and Applied Mathematics.

Hansen, P., 1992. Analysis of discrete ill-posed problems by means of the l-curve. Siam review (34), 561–580.

Harris, N., Pearce, J., Tindle, A., 1986. Geochemical characteristics of collision-zone magmatism. Geol. Soc. Special Publ 19, 67–81.

Hawke, P., 2004. The geophysical signatures and exploration potential of australia's meteorite impact structures. Ph.D. thesis, IUniversity of Western Australia.

Hidebrand, A., Penfield, G., Kring, D., Pilkington, M., Camargo, Z., Jacobsen, S., Boynton, W., 1991. Chicxulub crater: A possible cretaceous-tertiary boundary impact crater on the yucatan peninsula, mexico 19, 867-871. Tech. rep.

Koeberl, C., 1997. Impact cratering: The mineralogical and geochemical evidence. in: Johnson, k.s., campbell, j.a. (eds.), ames structure in northwest oklahoma and similar features: Origin and petroleum production 1995 symposium. Oklahoma Geological Survey Circular vol. 100, 30,54.

Koeberl, C., 2001. The sedimentary record of impact events. in: Peucker-ehrenbrink, b., schmitz, b. (eds.), accretion of extraterrestrial matter throughout earth's history. Kluwer Academic-Plenum Publishers, New York, NY, 333,378.

Koeberl, C., 2002. Mineralogical and geochemical aspects of impact craters. Mineralogical magazine, 745,768.

Koeberl, C., Farley, K., PeuckerEhrenbrink, B., Sephton, M., 2004. Geochemistry of the end-permian extinction event in austria and italy: no evidence for an extraterrestrial component. 32, 1053Ű1056. Tech. rep.

Koeberl, C., Shirey, S., 1991. ReŰos isotope systematics as a diagnostic tool for the study of impact craters and ejecta 132, 25,46. Tech. rep.

Langenhorst, F., 2002. Shock metamorphism of some minerals: basic introduction and microstructural observations. Bulletin of the Czech Geological Survey 3 (77), 265,282.

Lawson, C., Hanson, R., 1974. Linear least squares with linear inequality constraints. solving least squares problems. Tech. rep.

Li, Y., Oldenburg, D., 1996. 3d inversion of magnetic data. Geophysics (61), 394,408.

Ludka, I., Wiedemann, C., Töpfner, C., 1998. On origin of incompatible elements in the venda nova pluton, state of espírito santo, southeast brazil. South Am Earth Sci (11), 473,486.

Ludka, I., Wiedemann-Leonardos, C., Medeiros, S., Mendes, J., Moura, J., 1965. The extraterrestrial origin of canadian craters. Annals of the New York Academy of Sciences (123), 941,969.

Ludka, I., Wiedemann-Leonardos, C., Medeiros, S., Mendes, J., Moura, J., 2000. Arquitetura de plútons zonados da faixa araçuaí-ribeira. Geonomos (8), 25,38.

Medeiros, S., Mendes, J., McReath, I., Wiedemann, C., 2003. U-pb and rb-sr dating and isotopic signature of the charnockitic rocks from várzea alegre intrusive complex, espírito santo, brazil. South American Symposium on Isotope Geology, 609,612.

Medeiros, S., Wiedemann, C., Vriend, S., 2001. Evidence of mingling between contrasting magmas in a deep plutonic environment: the example of várzea alegre in the pan africa-brasiliano mobile belt in brazil. Academia Brasileira de Ciências (73), 99,119.

Mello, F., 2011. Petrografia e geoquímica do complexo charnockítico de aimorés: Um exemplo nde plutônismo pós-orogênico do cinturão araçuaí ribeira. Ph.D. thesis, USP.

Melosh, H., 1989. Impact Cratering: A Geologic Process. Oxford University Press, New York.

Mendes, J., McReath, I., Wiedemann, C., Figueiredo, M., 1997. Charnoquitóides do maciço de várzea alegre: um exemplo de magmatismo cálcio-alcalino de alto k no arco magmático do espírito santo. Rev. Brasileira de Geociências (27), 13,24.

Mendes, J., Wiedemann, C., McReath, I., 1999. Conditions of formation of charnockitic magmatic rocks from the várzea alegre massif, espírito santo, southeast brazil. Rev. Brasileira de Geociências (29), 47,54.

Nalini, H., 1997. Caracterization des suites magmatiques néoprotérozoiques de la région de conselheiro pena et galiléia. Ecole Nationale Supérieure des Mines de Paris et de Saint Etienne - PhD thesis, 237.

Nalini, H., Bilal, E., Correia-Neves, J., 2000. Syncollisional peraluminous magmatism in the rio doce region: mineralogy, geochemistry and isotopic data of the urucum suite (eastern minas gerais state, brazil). Revista Brasileira de Geociências 30, 120–125.

Oldenburg, D., 2005. Inversion for applied geophysics: A tutorial. University of British Columbia.

Parker, R., 1994. Geophysical Inverse Theory. Princeton University Press.

Pearce, J., 1996. Sources and settings of granitic rocks 19, 120–125.

Pedros-Soares, A., Leonardos, O., Ferreira, J., Reis, L., 1996. Duplo regime metamórfico regional na faixa araçuaí, uma reavaliação à luz de novos dados. Congresso Brasileiro de Geologia Anais, 6 (39), 5–8.

Pedrosa-Soares, A., Alkmim, F., Tack, L., Noce, C., Babinski, M., Silva, L., Martins-Neto, M., 2008. Similarities and differences between the brazilian and african counterparts of the neoproterozoic araçuaí-west congo orogen. Geological Society, London, Special Publications (294), 153,172.

Pedrosa-Soares, A., Campos, C. D., Noce, C., Silva, L., Novo, T., Roncato, J., Medeiros, S., Castañeda, C., Dantas, G. Q. E., Dussin, I., Alkmim, F., 2011a. Late neoproterozoic cambrian granitic magmatism in the araçuaí orogen (brazil), the eastern brazilian pegmatite province and related mineral resources. Geol. Soc. Lond. Spec. Publ (350), 25,51.

Pedrosa-Soares, A., Campos, C. D., Noce, C., Silva, L., Novo, T., Roncato, J., Medeiros, S., Castañeda, C., Dantas, G. Q. E., Dussin, I., Alkmim, F., 2011b. Late neoproterozoicŰcambrian granitic magmatism in the araçuaí orogen (brazil), the eastern brazilian pegmatite province and related mineral resources. Geol. Soc. Lond. Spec. Publ (350), 25,51.

Pedrosa-Soares, A., Castaneda, C., 2006. Magmatismo e tectônica do orógeno araçuaí no extremo leste de minas gerais e norte do espirito santo. Geonomos (14), 97,111.

Pedrosa-Soares, A., Leonardos, O., Ferreira, J., Reis, L., 1996. Duplo regime metamórfico na faixa araçuaí: Uma reinterpretação à luz de novos dados. In: SBG (Ed.), Congresso Brasileiro de Geologia , Salvador. SBG, Anais v. 6. Springer International Publishing, pp. 5,8.

Pedrosa-Soares, A., Noce, C., 2007. Orogeno aracuai: sintese do conhecimento 30 anos apos almeida 1977. Geonomos 15, 1–16.

Pedrosa-Soares, A., Noce, C., Wiedemann, C., Pinto, C., 2001. The araçuaí-west- congo orogen in brazil: an overview of a confined orogen formed during gondwanaland assembly. Precambrian Res (110), 307,323.

Pedrosa-Soares, A., Vidal, P., Leonardos, O., Brito-Neves, B., 1998. Neoproterozoic oceanic remnants in eastern brazil: Further evidence and refutation of an exclusively ensialic evolution for the araçuai west congo orogen. 26, 519–522.

Pedrosa-Soares, A., Wiedemann-Leonardos, C., 2000. Evolution of the araçuaí belt and its connection to the ribeira belt, eastern brazil. in: Cordani, u.g., milani, e.j., thomas filho, a., campos, d.a. (eds.), tectonic evolution of south america. CPRM, 265,285.

Pilkington, M., Grieve, R., 1992. The geophysical signature of terrestrial impact craters. Geophysics (30), 161,181.

Pilkington, M., Hilderbrand, A., Ortiz-Aleman, C., 1996. Gravity and magnetic field modeling and structure of the chicxulub crater mexico. Journal of Geophysical Research (99), 13147,13162.

Pinto, C., 2008. Folha jequitinhonha. programa geologia do brasil, cprm. Folha, CPRM Serviço Geológico do Brasil, Rio de Janeiro.

Pinto, C., Drumond, J., Féboli, W., 1997. Mapemaneto 1:500000 etapa i. Projeto leste - geologia nota explicativa do mapa inteiro, 161.

Pinto, C., Drumond, J., Féboli, W., 2001. mapeamento conselheiro pena e sao gabriel da palha. Tech. rep., CPRM , COMIG.

Pitcher, W., 1993. The nature and origin of granite, 321p.

Pleiscia, J., 2003. Application of gravity data to understanding impact mechanics. in impact cratering: Bridging the gap between modeling and observations. Abstract 8051, lpi contribution n 1155, Lunar and Planetary Institute, Houston.

Queiroga, G., Pedrosa-Soares, A., 2009. Folha nova venécia. programa geologia do brasil. Tech. rep., CPRM Serviço Geológico do Brasil.

Roberts, M., Clemens, J., 1993. Origin of high-potassium, calc-alkalic, i-type granitoids. Geology 21, 825–828.

Sampaio, A., Martins, A., 2004. Projeto extremo sul da bahia: Geologia e recursos minerais. in: Serie arquivos abertos da companhia bahiana de pesquisa mineral, salvador, 19. Tech. rep., CPRM Serviço Geológico do Brasil.

Schmidt, P., Williams, G., 1996. Paleomagnetism of the ejecta-bearing bunyeroo formation, late neoproterozoic, adelaide fold belt, and the age of the acraman impact. Earth and planetary science letters (144), 347,357.

Silva, J., Lima, M., Veronese, V., Junior, R. R., Júnior, O. S., 1987. Geologia, folha se.24 rio doce. rio de 16 janeiro, ibge, projeto radam brasil, levantamento de recursos naturais, v. 34. Tech. rep., IBGE.

Silva, L., McNaughton, N., Armstrong, R., Hartmann, L., Fletcher, I., 2005. The neoproterozoic mantiqueira province and its african connections. Precambrian Research 136, 203–240.

S.Medeiros, Wiedemann, C., Mendes, J., 2000. Post-collisional magmatism in the araçuaí-ribeira mobile belt: geochemical and isotopic study of the várzea alegre intrusive complex (vaic), es, brazil. Rev. Brasileira de Geociências (30), 30,34.

Trefil, J., Raup, D., 1990. Crater taphonomy and bombardment rates in the phanerozoic. Journal of Geology (98), 385,398.

Trompette, R., 1994. Geology of western gondwana (2000-500 ma). pan-african-brasiliano ggregation of south america and africa, 350p.

Whittington, A., Connelly, J., Soares, A. P., Marshak, S., Alkmim, F., 2001. Collapse and melting in a confined orogenic belt: preliminary results from the neoproterozoic aracuai belt of eastern brazil. AGU Fall Meeting, Abstract T32B 089. American Geophysical Union (82), 1181,1182.

Wiedemann, C., 1986. The evolution of the early paleozoic, late to post collisional magmatic arc of the coastal mobile belt, in the state of espírito santo, eastern brazil. An. Academia Brasileira de Ciências, (65), 163,181.

Wiedemann, C., 1993. The evolution of the early paleozoic, late to post collisional magmatic arc of the coastal mobile belt, in the state of espírito santo, eastern brazil. An. Academia Brasileira de Ciências, (65), 163,181.

Wiedemann, C., Medeiros, S., Ludka, I., Mendes, J., Moura, J., Costa, R., 2002a. Architecture of late orogenic plutons in the araçuaí ribeira fold belt, southeast brazil. Gondwana Res (5), 381,399.

Wiedemann, C., Medeiros, S., Ludka, I., Mendes, J., Moura, J., Costa, R., 2002b. Architecture of late orogenic plutons in the araçuaí ribeira fold belt, southeast brazil. Gondwana Res (5), 381,399.

Wiedemann, C., Mendes, J., Ludka, I., 1995. Contamination of mantle magmas by crustal contributions, evidence from the brasiliano mobile belt in the state of espírito santo, brazil. An. Academia Brasileira de Ciências, (67), 279,292.